UNIVERSITY OF CALIFORNIA
RIVERSIDE

A Study of the Catalysis of MoS_2 using Optical Photoluminescence

A Dissertation submitted in partial satisfaction of
the requirements for the degree of

Doctor of Philosophy

in

Materials Science and Engineering

by

Koichi Yamaguchi

September 2019

Dissertation Committee:

Dr. Ludwig Bartels, Chairperson
Dr. Christopher Bardeen
Dr. Harry Tom

The Dissertation of Koichi Yamaguchi is approved:

_____

_____

_____

Committee Chairperson

University of California, Riverside

ACKNOWLEGEMENT

Professor, Graduate and Undergraduate Students in Bartels lab, collaborators, funding agency, Material Sciences, Chemistry, Physics Professors, and Staffs at UC Riverside

People currently around

Ludwig Bartels	Advisor
Michelle Wurch	Editing - Organizing CVD Growth
Kortney Almeida	Figures - MoS_2 Film
Tom Empante	CVD furnaces

And not limited to, so many graduate and undergraduate students in the past and current

Thank you all

September 2019

Koichi Yamaguchi

ABSTRACT OF THE DISSERTATION

A Study of the MoS_2 Catalysis using Optical Photoluminescence

by

Koichi Yamaguchi

Doctor of Philosophy, Graduate Program in Materials Science and Engineering
University of California, Riverside, September 2019
Dr. Ludwig Bartels, Chairperson

Monolayer molybdenum disulfide (MoS_2) has many unique characteristics, one of which is a strong photoluminescence (PL) excitation due to its direct band gap property. Because of this characteristic, the surface morphologies can be inferred by studying the photoluminescence peak frequency and intensity. Regions where the surface is disrupted by changes in structural phase and defect density will be indicated by the PL fluctuations. We have investigated the hydro-desulfurization (HDS) catalysis using this MoS_2 response by widefield PL imaging. This wide field PL imaging technique has the advantage of shortening each acquisition time of a large sample area to 1-2 minutes instead of hours required for mapping scans. Within this time frame, surface morphology changes from temperature under a hydrogen environment and dosing a sulfur containing organic compound, benzenethiol, one studied in real time. We have also studied the reaction efficiency using gas chromatography (GC) with a mass spectrometer for the same condition as in the PL widefield imaging experiments. We have found PL activities in pre-HDS temperatures around 200°C to 300°C. In this temperature regime, there is PL enhancement due to defect density fluctuation. This

fluctuation gives extra clue for the status of defect density. Although the PL intensity gets small, there are some PL activities in HDS temperatures between 300°C to 400°C and little over this temperature. We have observed HDS conversion in this temperature regime as well as hydrogen sulfide (H_2S) on our GC system. It was not only edges but also the basal region which had PL intensity fluctuation. This activity may imply the HDS occurs in both the edges and the basal plane, contrary to previous beliefs that edges are the sole active catalytic sites.

Table of Contents

Chapter 4

List of Figures

Introduction

Among other transition metal dichalcogenides (TMDs), monolayer molybdenum disulfide (MoS_2) has been in the spotlight for its versatile new application for water splitting[1-11] and semiconductor devices[3-7]. Sulfur content must be lowered for fuel dispensed at gas station in order to reduce acid rain. MoS_2 is an earth-abundant cost-effective material which has been used for the hydro-desulfurization (HDS) process for several decades. The HDS process of MoS_2 requires a high pressure of over 150 atmosphere and temperatures between 260°C to 400°C. The study is limited to atomic-scale monolayer MoS_2 triangles grown in situ STM or TEM chambers[9-12-14]. The scale of the study is limited to ideal defect-free MoS_2 truncated triangle[15-19] in atomic size scales. The MoS_2 used in the industry is many layered and not under UHV conditions, therefore, the study is not close to the actual environment. If the processing temperature and pressure can be lowered, the cost and environmental effect can be greatly reduced for the HDS process. There are some benefits for knowing the mechanism of this catalytic process. The first step may be to try to study its property in the microscopic scale which is more realistic to industrial HDS processing than an atomic scale study. Monolayer MoS_2 has uniquely high photoluminescence due to its direct bandgap property[13 20-25]. A MoS_2 monolayer has 2H trigonal prismatic structure with two sulfur atoms both on the top and bottom and a molybdenum atom in the middle. Because of this crystal structure, it can be grown either in a triangle or hexagonal shape. We make MoS_2

triangular islands for this study by adjusting the sulfur to molybdenum ratio and growth temperature[26]. This is because the STM and TEM studies about HDS require atomic scale triangles to study its active edge structure. In order for the studies to be comparable, triangles with edges are used in this study.

When this monolayer structure is disturbed, the PL intensity fluctuates, and is directly corelated to surface defect density. We take advantage of this unique property to study surface defects on 2D MoS_2. We have developed a wide-field PL imaging system which can acquire images in short durations to study surface defect states. PL images are studied under a hydrogen gas environment for its temperature dependency evolution. Another experiment we have done is exposing the film at elevated temperatures in a hydrogen environment to see the pattern of PL under a cold state of around -100°C. Also, the dynamic state is observed under elevating temperatures. In both experiments, benzenethiol which has sulfur on a benzene ring is added to see the spatial information about the PL image. HDS conversion is monitored by both mass spectrometry and gas chromatography techniques. The correlation between PL images and gas chromatography is discussed.

Chapter 1 Wide Field Photoluminescence Microscope imaging of MoS_2 under Hydrogen atmosphere

1.1 Introduction

As the temperature of MoS_2 increases, the photoluminescence brightness decreases[27]. This is because bounded exciton pairs are dissociating by adding extra thermal energy. We initially start to observe experimentally this decrease in brightness due to a recombination process. If this is the only mechanism, the decrease should be monotonic. However, this was not the case in the region of the catalytically relevant temperature. There are many applications for MoS_2 catalysis, and in this study it is specifically for the hydro de-sulfurization (HDS) process. It is reported that a hydrogen environment induces an irreversible reaction on MoS_2 over 200°C[28]. Around this temperature, we see localized increase of PL intensity. These might be the indicative of MoS_2 catalytic activity as there might be some fluctuation of defect density.

1.2 Materials and Method

The monolayer MoS_2 samples used for the PL imaging experiment are CVD grown samples developed in Bartels lab[29]. We have chosen samples with triangles of 15 to 35 um features as the 40x microscope objective used for this experiment cannot

resolve any smaller triangles less than 10um length. Larger triangles are in general harder to grow using CVD process without compromising its single layer characteristic as it is prone to become bilayer. The samples need to be inside a chamber filled with hydrogen gas in order to create processing atmosphere. The viewport is in front of the sample and this will disrupt the optical path. A viewport-glass compensated microscope objective with long working distance is required to do optical imaging of the triangles inside a chamber. Some compromises have to be made using a lower magnification

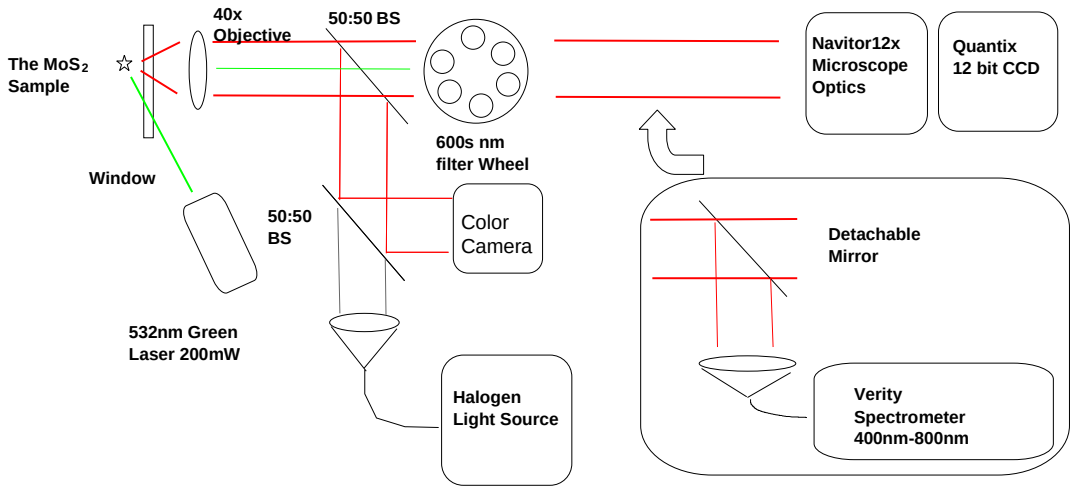

Figure 1 Overall schematics of experimental setup. It shows CCD sensor, 650-750 nm bandpass filter with 10nm width, USB color camera, white light, 532nm DPSS laser, Nikon microscope objective , and insertable mirror for verity spectrometer.

objective for gaining a longer working distance instead of using a high magnification objective for shorter working distance. Higher magnification resolves more features but requires shorter working distances. Using a view port requires long working distances.

Figure 2 Viewport, part of chamber with sample holder area, microscope objective

There are two versions for this set up. One with a heating element inside the chamber exposed to the process gases. The reaction may be taking place not only on the sample but on the heating element as well. The heating element may get much hotter than the sample stage and HDS may start taking place as a background rather than only at the surface of MoS_2 samples. Overall schematics of first version are shown on figure 1 and the sample holder with the viewport area is shown on figure 2 .

A liquid nitrogen flow cryostat LT3 (Advanced Research Systems) is attached to the sample holder via copper braiding. The cooling temperature is controlled by the same heater used to heat up the sample while flowing liquid nitrogen to the cryogenic cooling system. The vacuum of this chamber can be lowered to 1e-7 Torr range with a turbomolecular pump. A K-type thermocouple is secured onto the sample holder

assembly. Inficon combined compact ion gauges monitor both the main chamber pressure as well as the rough pump pressure.

There is an improved version of the set up in which the heating element is encapsulated inside the stainless-steel shielding and never exposed to the hydrogen, reactant nor products. The mini chamber on figure 3 consists of a viewport, inlet and outlet for reactive gas flow, and temperature sensor and actual picture is on figure 4.

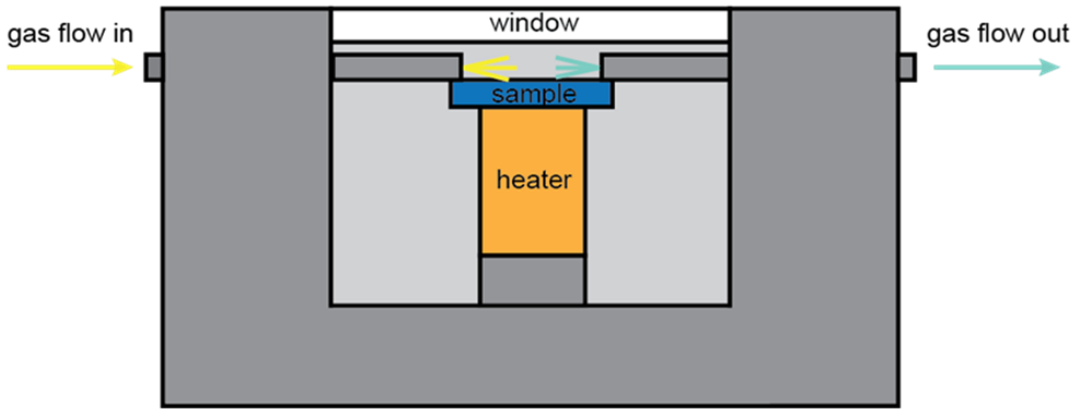

Figure 3 The mini chamber with heater assembly. (Second Version) Reactant mixture of Benzenethiol and Hydrogen flow on to the MoS_2 surface and Product is collected next to the sample and to the mass spectrometer.

We have used Watlow Firerod Cartridge heater ¼ inch diameter with 240V, 300W as a heater shown on figure 5. The heating element may get hotter than the sample holder, but it is not exposed to the reactive hydrogen gas and benzenethiol mixture as in the previous setup. This configuration extends the life of heating element as well as reduces the HDS background noise coming from the heating element and

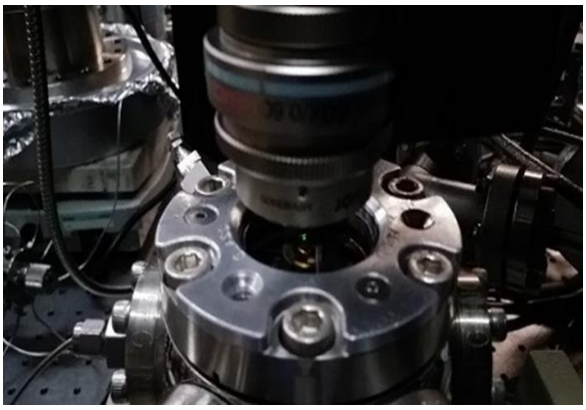

Figure 4 Reactive chamber in center, microscope seals chamber and objective on top are shown with gas connection

Figure 5 Sample holder assembly with ¼ outer diameter (OD), 240V, 300W Watlow cartridge heater. The sample holder is made of gold plated ½ inch OD molybdenum covering this heater assembly. ¼ Swagelok fitting seals gas tight connection to the ¼ NPT thread which seals chamber and ambient.

heating sample holder. The PL images are acquired via a -20°C cooled, 12-bit CCD camera KAF 1401E (Quantix, Photometrics). A Nikon infinity-corrected long working distance 40x, 0.6 NA objective is used to image sample surface. A 200 mm equivalent Nikon microscope tube lens is used for image projection to the CCD and also to the USB color camera for quick imaging. Overall schematics of the setup are shown on figure 6 a). Exposure for CCD imaging is typically 2 minutes with maximum gain of 3. In order to obtain spectral information, discretized bandpass filters are used. A 10 nm band-pass filter from 650 nm to 750 nm (Thorlabs FB series) are chosen and inserted into 7 of 8 positions filter wheel which a LabView program selects the appropriate filter for the experiment automatically. There are two methods employed to excite the MoS_2 film. One method is to illuminate sample at an angle from the side with 200 mW, 532 nm DPSS laser as seen on figure 7. One Plano convex lens with a focal length of 120 mm is situated approximately 120 mm away from the surface of the sample to focus laser beam.

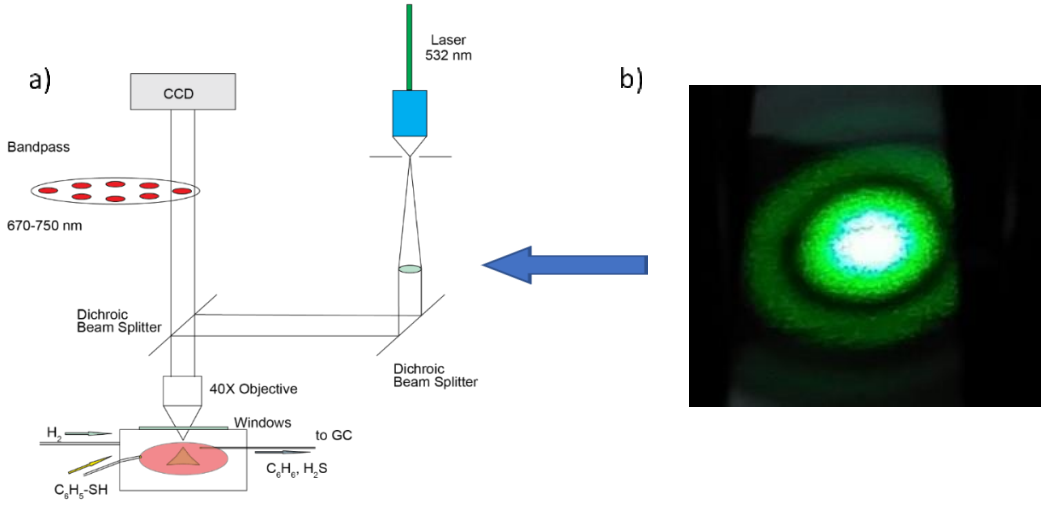

Figure 6 a) Simplified over all experimental set up of optics and mini reaction chamber. (Second Version) Laser assembly is directly mounted to the PL imaging system instead of side illumination. Spacial filter consists with 10x objective, 25um pinhole is used to clean up the laser beam. Best form lens with focus of 150mm to collimate diverging beam. CCD sensors with bandpass filters in front and 40x objective are shown as well as mini reaction chamber. b) A piece of paper is inserted between optical path to show the interference pattern. Blue arrow in figure a shows where paper is inserted. Center most clean portion is used to illuminate the sample surfaces.

Since a longer focal length lens is used to focus collimated light, the spot size is larger compared to the field of view of 40x objective with much shorter focal length. The laser shutter is in the middle of the optical path cutting laser light to prevent unnecessary exposure when it's not in the measurement. This side illumination method is simpler as there are less optical components the laser has to pass through. The laser produces coherent waves which can cause interference from imperfections on more optics. Side illumination limits optics to minimum and reduces interference patterns projected onto the sample is minimized. A coherent laser can produce higher

photoluminescence compared to LED sources and this method delivers enough power to excite the entire field of view of the sample. However, we later realized that the illumination intensity varied greatly even with small movement of the illumination position and thus precise photometrics measurements are not possible. Small movement of the laser position in a 10-micron range may causes unwanted fluctuation of laser power because of inhomogeneous illumination.

Figure 7 Picture of the optics setup along with direct mounted laser assembly, 3 axis spacial filter assembly, CCD sensor, 200mm Nikon tube lens, and filter wheel assembly are shown

The second version is epi-illumination where light passes though back of the microscope objective similar as in a typical metalogical microscope. This set-up is cleaner especially when using a white incoherent light source such as an LED. In order to produce strong PL for the experiment, an incoherent source is not enough. Therefore, a 500 mW laser (Torus, Quantum Laser) in the 532 nm range is chosen to illuminate the sample. The laser head is mounted directly onto the microscope assembly as seen in figure 8. The spatial filter assembly (Edmond Optics) consists of a 10x microscope objective, 15um pinhole and its mount with translation capabilities is between the laser optical path.

The spatial filter is cleaning up unwanted laser interference projected onto the sample plane. Homogenous illumination is achieved by this filter and also expands the beam size to match the back aperture of the Nikon objective. A best form lens with a focal distance the same as the distance from the pinhole is used to produce collimated light. In this case, a 150 mm focal length is chosen so that only a small portion of the first mode of Gaussian peak is used for the illumination. The first mode produced by the setup is shown on figure 6 b) and 8 by inserting a piece of paper before the collimating lens. A field stop is used to limit the diameter of the collimated light to match the back aperture size of the objective as well. Reducing the laser beam size prevents unwanted internal reflection inside the optics components. By having the spatial filter in place, and using the center-most diverged beam, homogenous excitation of the surface is possible without significant interference patterns. A collimated white LED light for illumination shares the same optical path as the collimated laser for color imaging. An aspherical lens with 100 mm is used to focus the collimated laser beam as well as the white light.

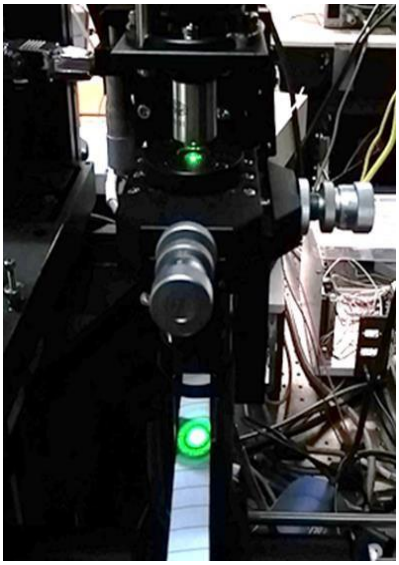

Figure 8 Two spots are illuminated green when the laser is turned on to show the interference pattern and spatial filter focusing point.

The sample is on top of the 0.5-inch diameter heating stage made of gold-plated molybdenum. Initially, the heating stage was made of oxygen free copper. The copper is found to be reactive under a hydrogen environment with benzenethiol. The surface of copper sample holder becomes black in the process. Thus, a new heating stage, composed of gold-plated molybdenum is used in the newer version. This sample stage is heated via a ¼-inch diameter, 1.5-inch length, 300W cartridge header (Watlow Firerod). The heater is controlled by an Omega Temperature Controller (CN32PT) with a solid-state relay. It is a USB-based controller which can be programed via LabVIEW. A K-type thermocouple is attached to the sample holder which provides temperature feedback to the sample holder. The heater controller allows it to maintain a constant sample temperature within +-1 degree accuracy. The reactant mixture (benzenethiol with a non-reactive gas such as argon) and hydrogen gas are premixed and delivered via a 20 mil ID, 1/16 inch OD stainless steel tubing and delivered right next to the sample in the reactive chamber as seen on figure 4. The reactant gas is pumped out via a rough pump with a back-pressure regulator set to 760 Torr. Further detail is discussed in chapter 2 mass spectroscopy.

Temperature dependent PL imaging is carried out up to 450°C with 50 degree stepping up from room temperature. PL images are acquired starting from 670 nm, 10nm bandwidth filter to 730nm filter and each acquisition is 1 to 2 minutes. A laser power of 160 mW is applied from the side illumination as

discussed earlier. Hydrogen gas flow with 500 sccm into the main chamber with total volume of 5000 cc chamber.

A grating spectrometer (Verity Instrument SD1024F) is placed in place of the CCD camera's optical path for measurement of PL spectrum as shown on figure 1. The temperature is set to ramp up to 200°C from room temperature and then to ramp back down to room temperature. Partial pressure of 150 Torr Hydrogen, and 600 Torr Nitrogen is achieved via a manual flow controller and exhaust flow balance. Total pressure of 750 Torr is maintained. Using the optical image as a guidance for focusing, a PL spectrum is acquired with the Verity 1024 grating spectrometer at each temperature.

LabView software does the image acquisition process semi-automatically. Prior to each acquisition set, either manual or auto focusing images with white light. The fast USB color camera is used to identify the image focus followed by re-focusing with a black and white camera. For the automatic focus routine, the brightness is maximized and the image is located in the focus position. A close-loop piezo actuator (Physic Instrument) sweep its absolute position with 100 um distance. While sweeping the microscope objective position, it acquires a series of images. Then it computes its mean brightness and records them. The mean brightness of the image is inversely parabolic with the position of the sample, and the peak brightness corresponds to the in-focus position. Both color camera and

PL imaging, Quantix camera are used for focusing. Both cameras show similar positions when the images are in focus. This extra step minimizes the offset of focal plane associated with two different sensors used for imaging. A bandpass filter is selected and the laser shutter is opened to excite the MoS_2 film. Then images are acquired for approximately 2 minutes depending on initial PL brightness. After the exposure, the laser shutter closes but the laser is kept on. The computer saves image files in TIFF format. The filter-wheel rotates to the next optical filter. The laser shutter is re-opened and exposure starts for the next image. This process is repeated for all the pre-chosen optical filters. The image position has some drift from one set of images to the other. Images are aligned on Mathematica for its shift associated with acquisition.

1.3 Results and Discussion

Initially the edge is bright with peak frequency at around 680 nm at room temperature as seen on figure 9 [30]. As the temperature increases, the red-shifting of PL frequency is observed[31-38]. This is to be expected due to the thermal expansion of MoS_2 on SiO_2 suspension. The mechanical strain by bending of the MoS_2 nanofilm exhibits a red-shifting effect on photoluminescence[39]. As temperature increases, thermal expansion causes the film to stretch its length. This is similar to the condition as applying mechanical tension. Initially, the PL intensity gets dimmer as increasing temperature up to 200°C. At temperatures

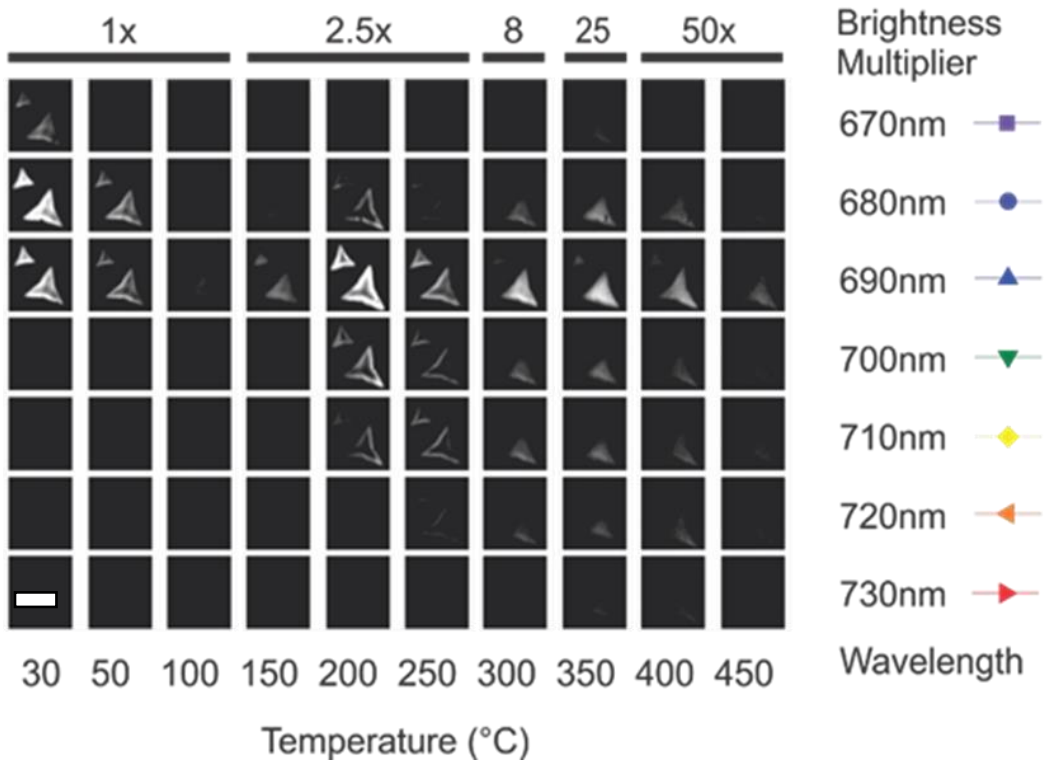

Figure 9 PL images of temperature dependency from room temperature to 450°C MoS_2 triangle under Hydrogen gas is shown. Intensity is amplified by the brightness multiplier indicated by the top bar and 670nm to 730nm in 10 nm bandwidth increment are shown. The scale bar is 15 um.

around 190-220°C, we have observed the recovery of PL intensity on both the edge and basal plane. The mean value of PL intensity is plotted which shows this recovery of PL intensity on figure 10 with 690nm as peak frequency. Peak frequency up to 200°C is plotted on the inset at top right side. In this temperature regime, defect density may have drastically increased due to movement of sulfur on the surface and edges. Research with STM and TEM on edges around this temperature confirms atomic-scale movement[13, 40-49]. PL intensity can be enhanced with increase in defect density[50-57]

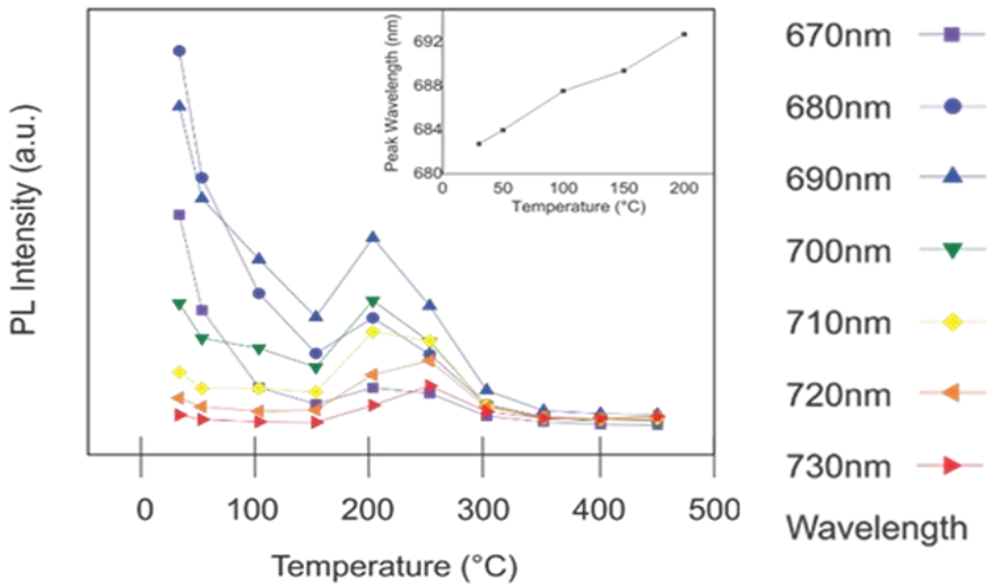

Figure 10 Mean brightness of the triangles corresponding to the figure a) are shown with peak wavelength with temperature red shifting is shown on inset. Since defect density increases with raising temperature, temperature is directly correlated with defect density. On top of standard decay of PL intensity, there is resurrected PL 200 to 300°C. Left side of this PL peak is denoted defect lean side and right side of this PL peak is denoted defect rich side and right around PL peak is denoted PL enhancement regime for discussion purposes.

especially on the edges. Our results shows PL enhancement recovery information on top of standard temperature decay of PL intensity due to recombination reduction. This recovery is very strong as PL intensity goes back up even from bottom of the standard decay curve between 200°C to 300°C.

Under a hydrogen environment, the red-shifting of PL continues to 690 nm but slows down even after elevating the temperature any further. Over 300°C the edge feature diminishes. However, the basal PL pattern remains and continues to get dimmer as temperature increases. The PL enhancement due to defects cannot continue at temperatures over 300°C. This is because PL enhancement may not

increase indefinitely due to the additional loss of material based on the shape in figure 10. The PL intensity continues to go back down and follows a standard decay profile with increasing temperature. As is mentioned earlier, the PL red-shifting does not continue further which is associated with the physical stretch of structure. Instead, sulfur begins to be able to move its position at temperatures over 200°C. As temperature increases, the number of defect sites increases. In a way, this figure shows the PL enhancement due to the defect density induced by temperature. In the following chapters, this peak relationship is used to identify the location of the defect density for each experiment.

Red shifting is observed on the spectrograph measurement as seen on figure 11 a) and the peaks go back to the original frequency as seen on b). Wide field PL imaging shows the spectrum redshift as seen on grating spectrometer up to 200°C. Epi-laser illumination at the back of the objective confirms similar traits to side illumination. Illumination becomes homogenous as the center most interference pattern is the only thing passing from the point to the sample as exciting source.

a)

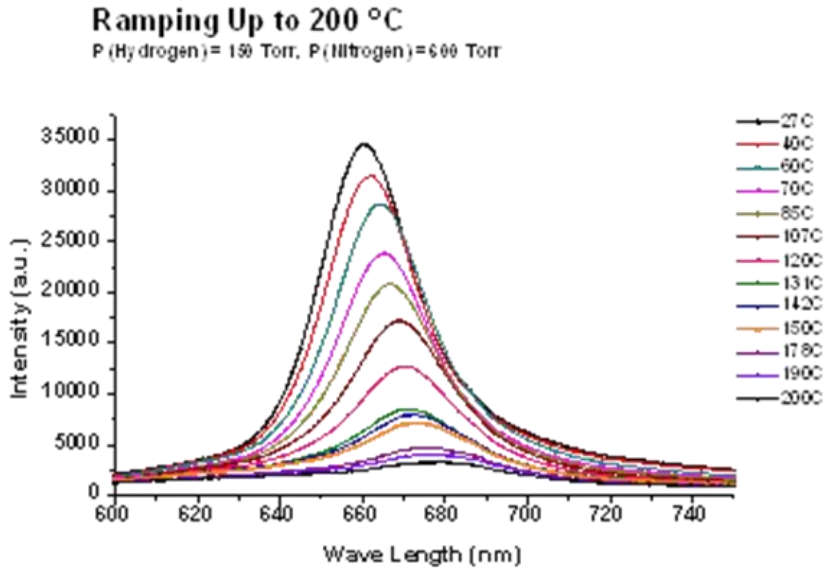

b)

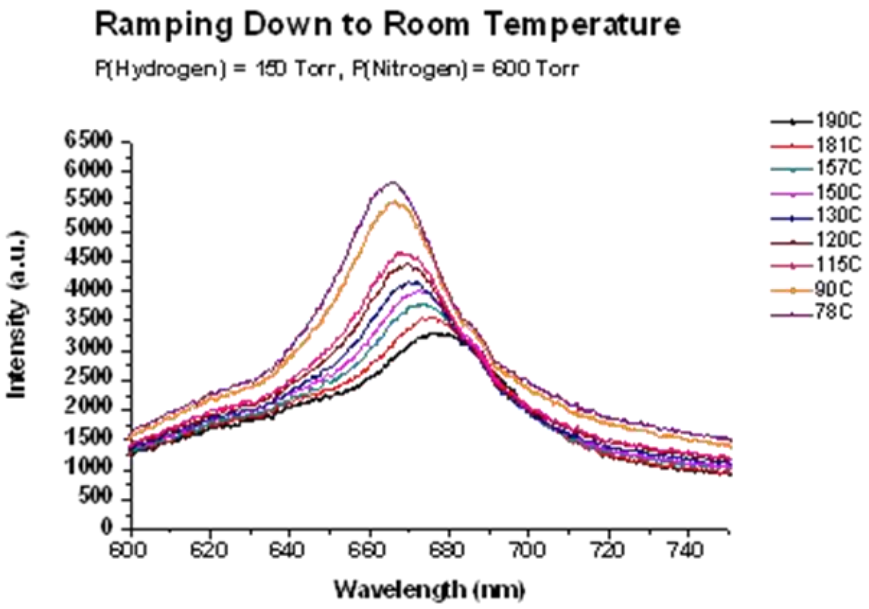

Figure 11 a) PL spectra using grating spectrometer (Verity SD1204) showing red shifting as temperature is ramping up to 200°C. b) PL spectra for ramping down to 78°C. Redshifted peak goes back to similar peak position comparing 85°C while maintaining constant flow of gas in and out with partial pressure of hydrogen is at 150Torr and nitrogen is 600 Torr.

Chapter 2 Mass Spectroscopy and Gas Chromatography

2.1 Introduction

There are photoluminescence activities with varying temperatures under a hydrogen environment as presented in chapter 1. The HDS conversion efficiency varies with each temperature regime. The correlation between the PL image evolution and HDS activity allows us to identify corresponding activities. The PL images contain spatial information about surface defect density of the material while the mass spectrum shows its conversion efficiency. Therefore, we have set up a mass spectrometer in order to sample the reactants and products in two different ways. One way is to continuously flow sampled gas into the mass spectrometer chamber. This method allows for real time monitoring. However, this method does not allow for baseline subtraction. The second way is using a gas chromatography technique with a column.

The sample gas is collected at fixed intervals and thus baseline subtraction is possible. Benzenethiol is ionized at the mass spectrometer adding additional aliased signals to the benzene measurement. This problem is isolated because the chromatographic peak separation isolates the benzene peak produced by the reaction chamber and the amount produced by benzenethiol.

2.2 Materials and Methods

The first method involves direct sampling. The gas sample is under a hydrogen gas environment while ramping up the temperature to the HDS active temperature in the reactive chamber. Sampling takes place continuously in the proximity of the MoS_2 film on SiO_2 through a 1 mm ID, 1/16-inch OD stainless steel tube. Since the amount of gas flow required to maintain HDS reaction in the main chamber is larger, the entire reactant cannot be fed into the mass spectrometer. This is because the pumping speed of the mass spectrometer cannot handle a large flow. The mass spectrometer chamber must maintain good vacuum pressure for the mass spectrometer to function correctly. The solution is to create an intermediate chamber and the method we have employed uses a setup similar to the "High Pressure Sampling" technique explained in Appendix B of the SRS residual gas analyzer manual. Most of the sample gas is pumped out via an oil-less rotary pump using adjusted flow. Only a small amount of the gas sample is needed for the mass spectrometer (RGA 200, Stanford Research system) and is acquired from the intermediate stage. The reactive chamber is maintained at approximately 760 Torr and the intermediate stage is maintained at approximately 10 mTorr. Benzenethiol (C_6H_5-SH) is continuously dosed while the mass spectrometer is set to monitor benzene (C_6H_6) and hydrogen sulfide (H_2S) partial

pressures simultaneously. Hydrogen gas flow is maintained between 5 to 50 Standard Cubic Centimeters per minute (sccm) and the nitrogen bubbler flow is also maintained between 5 to 50 sccm, depending on the desired mixture ratio. In this instance we have chosen 10 sccm for hydrogen flow and 7 sccm for the argon bubbler gas. The MoS_2 sample is on the PID-controlled heating stage controlled by Labview PID package. A K-type thermocouple gauge is attached to the sample holder which provides temperature feedback. The sample is heated from room temperature up to 450°C. A sample with MoS_2 triangular islands grown using the CVD method mentioned in Chapter 1 is used to take PL images while ramping up the temperature. Since each imaging acquisition and focus takes several minutes, PL images are taken without bandpass filters except a 532 nm lowpass filter which removes strong laser scattering.

Simultaneously, a mass spectrum is acquired continuously.

Temperature is maintained at 210°C, 225°C, 245°C, 270°C, 300°C, 330°C and 360°C for the MoS_2 film mentioned and at each hydrogen-nitrogen concentration ratio dosed. Benzene (mass 78) and benzenethiol (mass 110) are monitored in a continuous method by mass spectrometry mentioned in the earlier paragraph. For each measurement, the sample films are cut into similar dimensions. Usually a single sample can be cut into four equivalent sizes. Nitrogen gas flow for bubbling benzenethiol is maintained at a constant flow rate. In the next experiment, a 30% hydrogen-nitrogen mixture is maintained, and

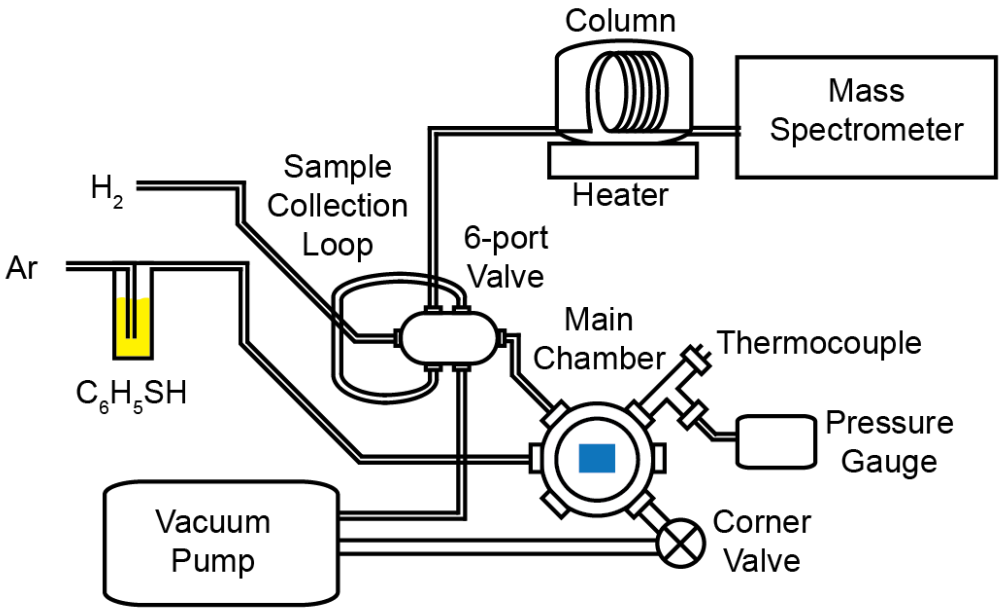

Figure 12 Micro Reaction Chamber on the center with Gas Chromatography setup: consists of 6 port injection valve with 60 uL sample loop, GC gas column, K type Temperature connection , Pressure gauge, and Corner valve. Hydrogen and Argon gas bubbler are controlled by Mass flow controller not shown.

temperature is held for 270°C, 300°C, 330°C, 360°C, 365°C, 390°C and 420°C. Each sample uses the same ramping profile rate of 10°C per minute.

The second method uses a gas chromatography technique instead of direct sampling the reactive chamber gas. The overall setup of this experiment is shown in figure 12 and consists of a micro reactive chamber with a viewport placed in the middle of the diagram. Since benzenethiol is ionized and produces a benzene signature on the filament of the mass spectrometer, it is difficult to quantify the number of reactants and products that come from the actual sample. Benzene signal can be produced at the ionizer on the mass spectrometer from the benzenethiol. The more reactants there are, the more product will be shown on

the mass spectrometer, which might not be related to HDS conversion on the sample itself.

With the gas chromatography method, the system can separate the number of reactants and products by time separation with a delay of peaks. Using a computer controlled sampling valve, with 2 positions, 6 injection ports (Valco Instruments Company Incorporated), 60 uL of gas is sampled from the main chamber in a repeatable fashion and inject into GC column (GsBP-1 29 meter, 0.25ID, 1um). A solenoid valve is controlled electrically by opens and closes the pneumatic actuator connected to the 6-port valve. The repetitive sampling with 5 seconds at 10-minute intervals is achieved via a LabVIEW-controlled program. This 6-port valve also injects the sampled gas into the column followed by the mass spectrometer chamber. A mass-flow controller maintains its flow rate between 1 to 2 sccm, which is enough to maintain good mass spectrometer chamber pressure better than $1x10^{-5}$ Torr. The column is heated to 240°C isothermally so that each sampling is complete within 10-minute sampling intervals. This time is chosen because benzenethiol detection requires a longer time as compared to benzene and hydrogen sulfide. This is because it has a slow traveling speed, yet it is within the 10-minute experimental intervals. The temperature of the sample is programmed to ramp up and down at fixed intervals and the sampling of the reacting gas takes place with fixed intervals as well.

First, we acquire a baseline mass spectrum by performing the experiment procedure on a dummy SiO_2 sample containing no MoS_2. The sample holder, made of gold evaporated molybdenum, can be a source of an aliased reaction site. Therefore, the SiO_2 blank sample with 12 mm x 12 mm size is used to collect its background signal. Placing this dummy substrate covers the metal surface of the sample holder, minimizing an aliased HDS conversion. A 2 mm ID, 1/16-inch OD stainless steel tubing is used to deliver a hydrogen and benzenethiol-argon mixture. The mixture of benzenethiol-argon is premade by bubbling argon gas through benzenethiol liquid. The tip of this nozzle is aimed toward the top of the sample so that the majority of the reaction takes place on the sample surface. The reaction chamber internal volume is approximately 74 cc. The hydrogen gas flow rate is chosen so that most of the reacted gas is replaced within the experimental sampling interval. When the hydrogen flow is 7.4 cc per minute, fresh hydrogen will fill the entire chamber volume every 10 minutes, thus flushing the entire chamber within the sampling period.

The vapor pressure of benzenethiol is 1.4 mTorr at 20°C and the argon which bubbles through is 760 Torr, so approximately 0.18% of the argon mixture by volume contains benzenethiol. And the flow rate for the argon varies from 5 sccm to 20 sccm. The blank sample is replaced with an MoS_2 film grown in our lab[58] . We have performed the exact same temperature measurement with the same gas flow and chamber pressure as for the blank sample. The sample is

programed to ramp up by 2°C per minute and is sampled every 10 minutes. Therefore, the signal is acquired for every 20°C steps and for 5 second durations. Subsequently, the background signal is subtracted for mass 78 (benzene) and mass 34 (hydrogen sulfide), with each peak amplitude determined by gaussian peak fitting.

Benzenethiol is bubbled through a mass flow controller with argon gas as a bubbler gas at 30 sccm to detect mass 110. Higher masses are harder to detect so the sampling duration is set to 5 seconds before sampling and 1 second after sampling. This is necessary to detect benzenethiol on the mass spectrometer. Otherwise, a continuous flow of Benzenethiol-Argon mixture as half or equal to the hydrogen gas flow into the chamber is enough hydrogen concentration for the experiment. Benzene and hydrogen sulfide are detected without detecting benzenethiol on the mass spectrum.

2.3 Results and Discussion

When the temperature increases over 270°C, hydrogen sulfide starts to increase its signal, as seen in figure 13 and when the temperature reaches just under 390°C, the steepness increases. For the HDS reaction to take place continuously, hydrogen sulfide must be produced based on the chemical reaction shown in equation 2.1 below.

$$C_6H_6S \text{ (Benzenthiol)} + H_2\text{(Hydrogen)} = C_6H_6 \text{ (Benzene)} + H_2S \text{ (Hydrogen Sulfide)}$$
(MoS_2 as Catalyst) Eq 2.1

Hydrogen sulfide is indeed detected under a hydrogen environment within the HDS relevant temperature. PL imaging shows pronounced edge feature starting to disappear over 350°C as seen in figure 2.4-1 b). The defect density increases which intensifies PL at room temperature as studied in past research[50]. We have occasionally observed enhancement of PL intensity around 250°C under a hydrogen gas environment. However, the dimming of PL intensity with increasing temperature may be attributed to a decrease in radiative recombination. It could potentially be an increase in defect density past the point of the PL enhancement effect.

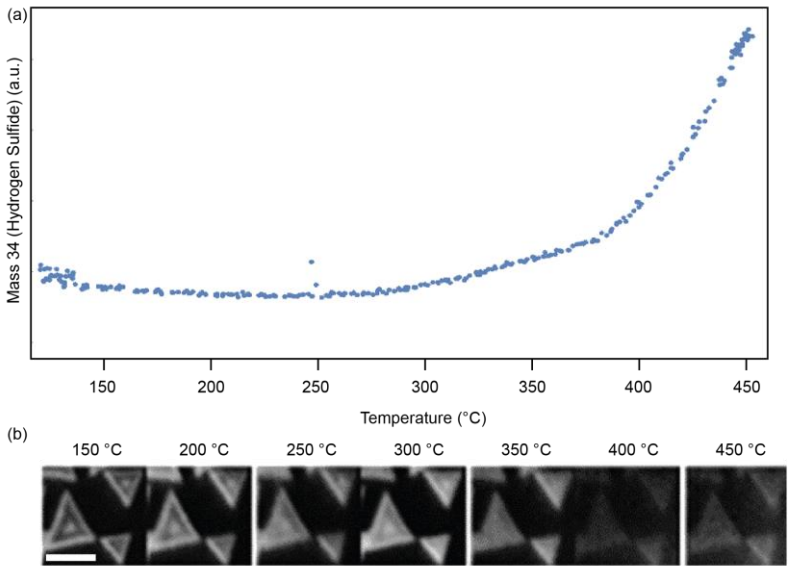

Figure 13 Mass spectrum for mass 34 corresponding to Hydrogen Sulfide (H_2S) on a) with transition temperature of 260 and 390°C. This signal is including both sample reaction as well as sample holder. The corresponding PL image of this reaction is shown on b) with pronounced feature gone at 350°C and noticeable dimming over 400°C. The continuous flow of Hydrogen and exhausting reactant at the same rate to maintain 760 Torr. Measurement is taken in the first version setup. The scale bar is 15 um.

At a 360°C holding temperature and with a 30% hydrogen, 70% nitrogen mixture, the HDS conversion efficiency is peaked as seen in figure 14 a). At temperatures below 360°C, the conversion peak at 30% hydrogen concentration is not observed. Similarly, over 360°C, the HDS reaction is sustainable for a 6 to 8 hour period at higher temperatures. Below this temperature, the reaction starts to decrease over time as seen in figure 14 b). This indicates that the desorption rate is not fast enough to catch up to the adsorption rate below this temperature. The continuous method has a bias in methodology. The copper sample holder surface and hot heating element act as a reaction sites in addition to the sample itself; this metal surface may however become inactive because it becomes coated with black reacted material. This may also be reducing the apparent HDS reaction over time. Whereas, the MoS_2 film surface is not affected by the blackening effect taking place on the copper metal surface. Because of this reaction on the surface of copper, the reaction associated with these surfaces may diminish over time especially at such low temperatures compared to metal catalysis. Bulk MoS_2 is known to be HDS active over 300°C and up to 425°C as a hydrocracking catalyst. Therefore, the only continuous reaction may be a response from the MoS_2 film.

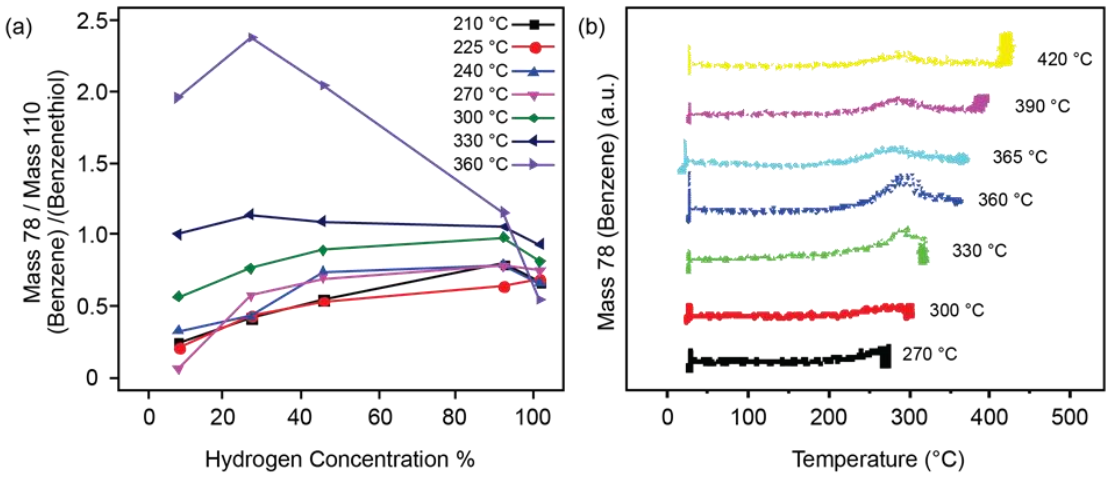

Figure 14 (a) HDS reaction rate is shown at different temperature with different Hydrogen concentration as shown. Some of the reaction may come from sample holder and sample on the film. 30% hydrogen concentration at 360°C shows highest activities.

(b) It shows benzene concentration decrease or increases as ramping up and holding temperature. Over 365°C, the Benzene concentration is maintained without decreases as temperature increases. Lower than this temperature, the benzene concentration starts to decrease over time. Measurement is taken with the first version setup which uses copper sample holder. Some of the Benzene may be produced on this copper surface consuming the metal. Temperature is not high enough to sustain copper surface conversion. Whereas MoS_2 film is at the HDS reactive temperature to sustain reaction over 365°C.

The main chamber pressure and intermediate chamber pressure greatly affect the mass spectrum signal level. Since the mass spectrometer gives a fluctuating baseline every time there are slight changes in overall gas pressure, the interpretation of the data is limited. The background signal is hard to subtract from the overall signal. Therefore, there is no reference signal. Also, some of the conversion is taking place at the red-hot heater which is hotter than the actual sample temperature as mentioned previously. Therefore, we have approached this process with a different setup to overcome this problem.

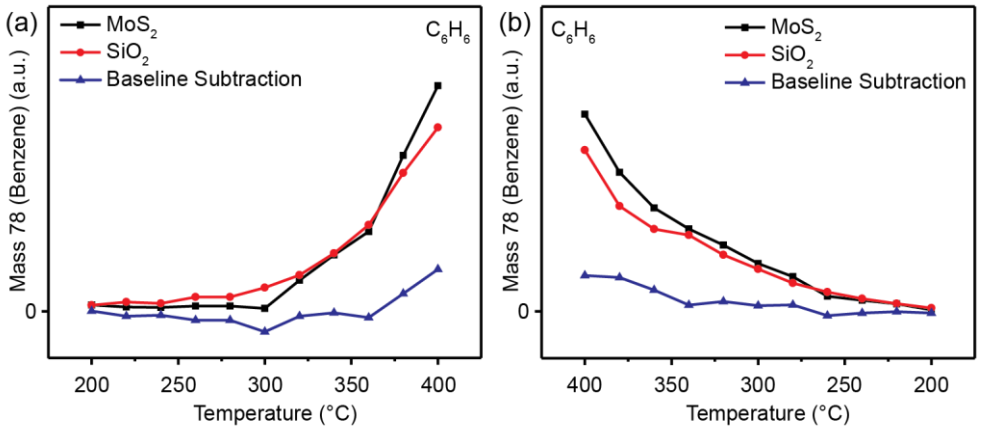

Figure 15 Benzene (Mass 78) concentration is going up and detected over 380°C on Gas Chromatographic experiment while ramping up as seen on a). Blue line shows the signal after the background is subtracted by the blank SiO_2 sample. The same background subtraction is applied on figure b) for ramping down. While ramping down, Benzene is detected till 360°C. Gas is sampled every 10 minutes and temperature ramping is 2 degree per minutes. Peaks are fitted and extracted from the raw data. Experiment is carried out in mini reaction chamber with gas chromatography.

The second experiment setup employs a gas chromatography (GC) column which overcomes several limitations encountered in the first design. With the second design using the GC technique, a baseline can be clearly separated from signal peaks. Because of the discretization of those data peaks. Since a GC column regulates gas flow for the mass spec, the baseline signal level becomes much more stable than continuous flow. Also, a background acquired by the dummy SiO_2 substrate can be subtracted from the signal. With both a stable signal and background subtraction, the system becomes much more sensitive to smaller signals. An SiO_2 blank-sample measurement shows the apparent HDS reaction from an elevated sample holder and heater assembly. Since the background becomes more sensitive, we have started noticing the sample holder being a large

contributor to the signal. A gold-plated molybdenum sample holder is used to reduce apparent HDS reactions.

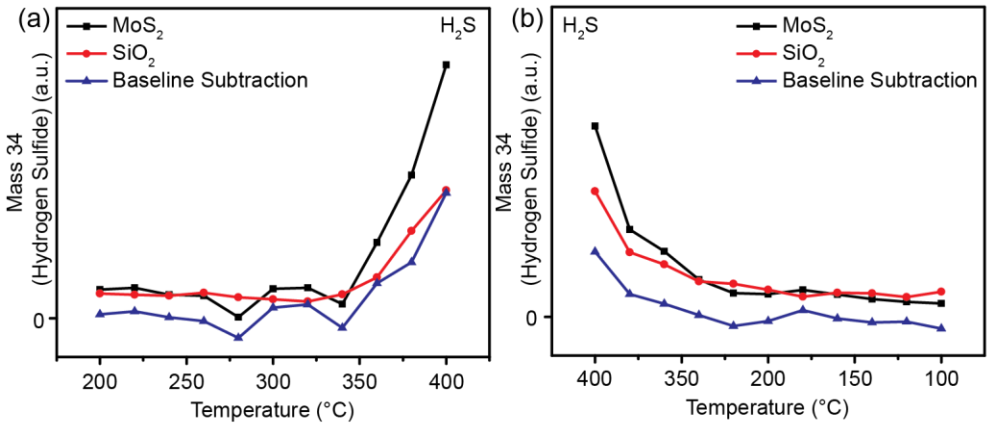

Figure 16 Hydrogen Sulfide (Mass 34) concentration is going up little earlier than Benzene concentration at 360°C on Gas Chromatographic experiment while ramping up as seen on a). Blue line shows the signal after the background is subtracted by the blank SiO_2 sample. The same background subtraction is applied on figure b) for ramping down. While ramping down, Hydrogen Sulfide is detected till 360°C the same temperature as ramping up. Gas is sampled every 10 minutes and temperature ramping is 2 degree per minutes. Peaks are extracted from raw data. Experiment is carried out in mini reaction chamber with gas chromatography.

The baseline (red) is subtracted from the MoS_2 film sample (Black) and the concentration for both benzene and hydrogen sulfide (both blue) are shown in figure 16. It becomes apparent at temperatures over 360°C that the benzene concentration starts to overcome SiO_2 dummy signal. A bit before 340°C, the hydrogen sulfide concentration starts to appear on the spectrum. If the sensitivities for both masses are similar, then it indicates the creation of defect sites prior to the active HDS catalytic temperatures. The ramping up and down concentration for both signal and background are slightly asymmetrical. However,

the baseline corrected conversion signal shows a symmetrical shape for both ramping up and down. There is more unreacted benzenethiol in the chamber while ramping up and less while ramping down. After background subtraction, it becomes the symmetric reaction for both cases. This finding shows a slightly higher HDS temperature which is contrary to the known HDS relevant temperature in STM and TEM scientific literature. Whereas, hydrocracking literature shows a similar temperature regime for their reaction study[59-62]. This experiment involves film which does not have active edge features that have been studied theoretically and experimentally[46, 63-65]. In the previous chapter, the PL images show its PL recovery around this lower temperature regime. There is some literature discussing PL intensity enhancement due to an increase in defect density[50, 51, 53, 54, 57, 66-70]. Coincidentally our PL imaging experiment also shows PL enhancement at a slower regime of HDS temperature. The defect density has drastically increased due to the edge activities which is indicated by an increase in PL brightness. As temperature increases further, the recombination rate decreases, and defect density increases beyond the point of PL enhancement and start to diminish over 300°C.

The Benzenethiol is constantly dosed however, raw data from mass spectrometer with chromatography is unstable due to the detection level as seen on figure 17. The signal gets smaller with heavier mass as compared to lighter masses. Smaller periodic peaks do not correspond to the benzenethiol as these

peaks coincide with larger argon peaks. Some secondary wider smaller peaks correspond to the dosing of benzenethiol. It shows a slightly higher concentration for SiO_2 than MoS_2 film. Benzenethiol has to travel on the surface of the substrate to be collected on the other side as seen in figure 18. Some portion may get converted to benzene as a response to the elevating temperature for MoS_2 (Black) and should not be reacted with SiO_2 surface (Red). Raw data without peak fitting for benzene is shown on figure 18 as a reference. In order to detect HDS activities at the lower temperature regime, a greater number of MoS_2 triangles with active edge sites may be needed in this setup.

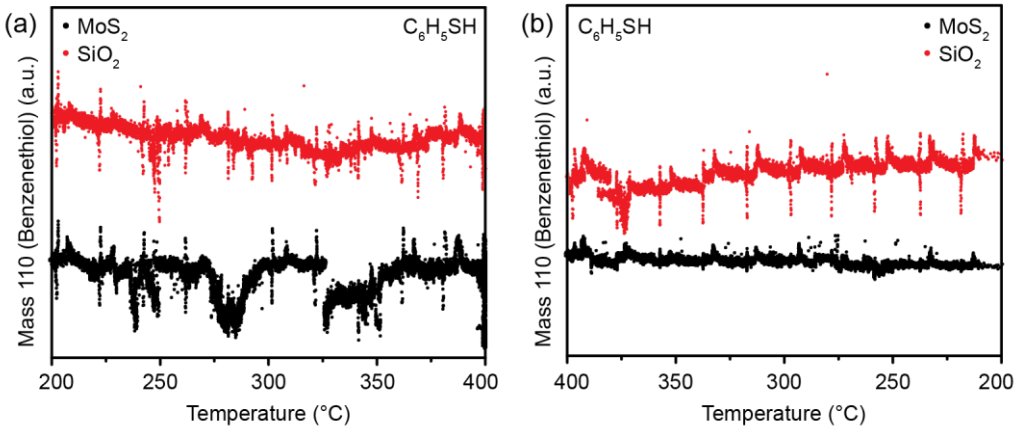

Figure 17 Raw data of Benzenethiol (Mass 110) concentration is shown while ramping up in a). Since Benzenethiol signal is at detection limit of the instrument, baseline of the signal is not stable. High sharp peak is aliased signal from Argon gas peak. The secondary wider peaks are corresponding to Benzenethiol dosing. Gas is sampled at every 10 minutes at 200, 220, 240, 260, 280, 300, 320, 340, 360, 380 and 400°C. Experimental requirement for dosing Benzenethiol may be lower than the detection limit of Mass Spectrometer. Therefore, sample becomes overdosing condition in order to see Benzenethiol dosing amount. Experiment is carried out in mini reaction chamber with gas chromatography.

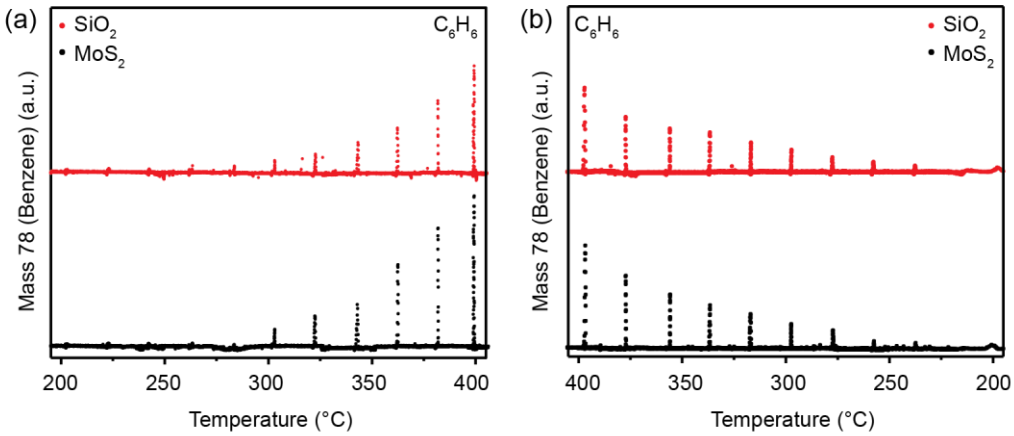

Figure 18 Raw data of Benzene without peak fitting for MoS_2 film in black and bear SiO_2 substrate in red which corresponding to figure 2.4-2 with ramping up in a) and ramping down in b). Experiment is carried out in mini reaction chamber with gas chromatography.

Chapter 3 PL Imaging at Frozen State (Room and -100°C) and Relevant findings

3.1 Introduction

PL imaging and gas chromatography show catalytic activity at HDS temperatures. Throughout the experiment, we have found interesting characteristics which may help to understand the mechanism relevant to HDS catalysis. In the first chapter, the temperature dependence of MoS_2 under a hydrogen atmosphere and corresponding PL images is discussed. For this chapter, we examine what happens at pre-HDS, and HDS active temperatures if MoS_2 monolayer films are heated up and maintained for a long period of time under a hydrogen environment. The PL measurement is performed at room temperature and at -100°C. The recombination rate is intrinsically higher at the latter because the lower temperature and PL images give more information about the internal structure.

3.2 Materials and Method

This PL imaging experiment is performed similar to the methods explained in chapter 1 for temperature dependent wide-field imaging. The difference in this method is that the temperature is maintained at elevated levels for 2 to 3 hours over the HDS temperature for each heating cycle. Then we wait for samples to cool down to room temperature and PL images are obtained. Again, the sample is

reheated to a high temperature for 2 to 3 hours, and this is followed by a cooling step for the PL measurement. We repeat the heating and cooling cycle for up to a total 21.5 hours. Fresh hydrogen gas is constantly flowed into the chamber at 50 sccm preventing the depletion of hydrogen gas due to consumption. The experiment is conducted in a 100% hydrogen gas environment.

In the next experiment, a more systematic experiment is carried out. A sample is heated up to 275°C, 325°C, 375°C, or 425°C and maintained at each for 2 hours before being cooled to -100°C. After each cooling step, PL imaging is performed at -100°C. The cooling is done with liquid nitrogen. After the PL imaging step, samples are reheated to the same temperature for an additional 2 hours and up to 20 hours exposure total.

For the last heating to 425°C step, the PL imaging is performed at this maintained temperature. This will give a PL image pattern at a dynamic state under hydrogen environment. For this sample, the PL intensity at -100°C is much lower as compared to that of samples processed only at cooler temperatures. Therefore, we stop processing any further after a 10-hour mark of sample lifetime. Since the PL intensity is much lower than of other samples, one extra step is carried out with this sample. We dose benzenethiol at 375°C to see what happens in the duration of 1 minute, 5 minutes, 5 minutes and 5 minutes. PL images are again acquired after cooling down to -100°C.

3.3 Results and Discussion

Since the measurement is taking place both at room temperature and -100°C, the defect density increases after elevating the temperature under a hydrogen environment which enhances the PL intensity. Initially, the PL intensity at the edge sites gets enhanced within the first 4.5 hours as seen on figure 28 at Appendices. The edge site is fairly active as reported in the previously mentioned STM and TEM studies at a little over 250°C (for edge sites only). At temperatures over 320°C under a 100% hydrogen environment and without dosing benzenethiol, the edge photoluminescence begins to shift inwards at the 10.5-hour mark as seen in figure 19 b). When further elevating the temperature, the edge moves inward as seen on figure 19 c). Destruction of the edge PL is observed prominently. However, the edge PL does not move further inward after this point. Instead, the entire PL gets dimmer and dimmer.

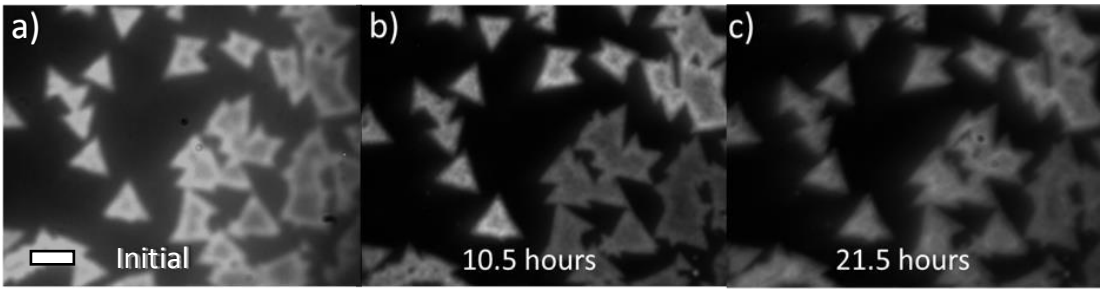

Figure 19 PL images of MoS_2 triangles, measured at room temperature, a) initial condition, b) after 10.5 hours under hydrogen exposure at 760 Torr 320-360C, c) 21.5 hours Total time. Edge of PL brightness has moved in word from initial condition and further exposing under Hydrogen environment. Brightness between initial condition a) are different scale from b) and c). The scale bar is 15 um.

Comparing the edge PL of shorter and longer wavelength, shorter wavelength moved further inward than longer wavelength as seen on figure 28 after 15 total hours. Since shorter wavelength is associated with smaller structure for MoS_2 with higher energy, more defect of smaller size is present on inner perimeter. Whereas, longer wavelength corresponding to lower energy with larger structure, larger size defect is at outer perimeter. One can predict that defects are propagating toward the center from the outside in needle like shape and fewer defects exists at basal plane at room temperature.

Interestingly, red-shifting of peak frequency is permanent in the PL images observed even measurement is performed at room temperature for this sample processed over 300°C. Red-shifting is reversible up to 200°C as discussed in the spectrometry results in chapter 1. Reversible here means comparing between red-shift of PL peak with a pristine (unprocessed) sample at room temperature and after heating up to 200°C under hydrogen gas environment. The amplitude of the peak has been decreased but the position of the PL peak goes back to its original frequency as seen in figure 11. This PL spectroscopy is measured at each temperature without cooling down in between each temperature. The initial data point is at room temperature and the final temperature is around 80°C as cooling takes a longer time to reach room temperature. The temperatures between 200°C and 275°C is where the irreversible red-shift occurs and coincidentally, the local PL enhancement takes place at 200°C.

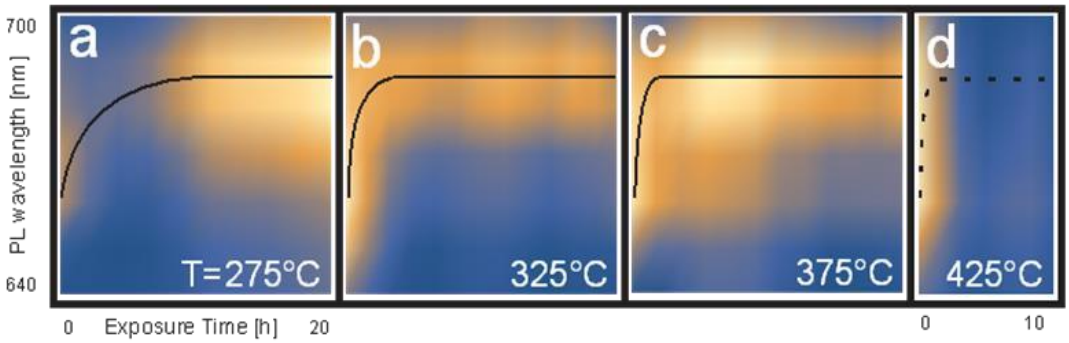

Figure 20 Hydrogen Annealing effect of MoS2 with four different temperatures: 275, 325, 375, 425°C for a), b), c), d) respectively. PL intensity plot are taken at -100°C for enhancing PL images of triangles. Annealing pressure is 730 Torr and PL imaging is 1e-5 Torr or lower.

For the next experiment, we performed an even more systematic approach with regards to temperature and interval duration. All the samples except at 425°C are permanently red-shifted when measured both at room temperature and -100°C. The mean intensity of triangles processed at 275°C, 325°C and 375°C all show red-shifting of the spectrum for both at room temperature and -100°C and the PL intensity plot is shown in figure 20 for -100°C. Initially, the PL intensity diminishes and then there is PL recovery with red-shifting from the peak position of 670-680 nm to 690 nm. At 275°C, the PL enhancement takes longer as it requires the defect density to increase from a pristine sample. This red-shifting is maintained with PL imaging at room temperature and at -100°C. This red-shifting memory effect may suggest some structural changes such as slipping of atoms between the film and substrate, phase change, adsorption of hydrogen atoms at vacancy sites, or adsorption of dissociated hydrogen. Red-shifting occurred for this set of samples just as it had in the previous experiment however, the edge

erosion is not present in this set of samples. It may simply have to do with the stability variance of CVD-grown samples. It may need longer processing time to see the similar erosion seen from the first experiment.

For the sample processed at 425°C, the PL brightness is much lower than compared to lower-temperature processed samples even when the samples are cooled and measured at -100°C. At the 10-hour hydrogen exposure mark, we stop carrying out hydrogen heating. The sample temperature is raised to a lower temperature of 375°C and not 425°C. Benzenethiol is dosed at 1-minute time intervals and therefore initiates PL recovery with red-shifting as seen in figure 20. Further cycles of benzenethiol dosing at 375°C with 5-minute intervals shows a steady increase in PL brightness up to a certain point. Depending on the defect density site, the PL enhancement profile differs. PL gets brighter or dimmer by repairing the structure of the defect sites. If the sample is at a defect rich side of profile, then dosing benzenethiol makes the PL brighter.

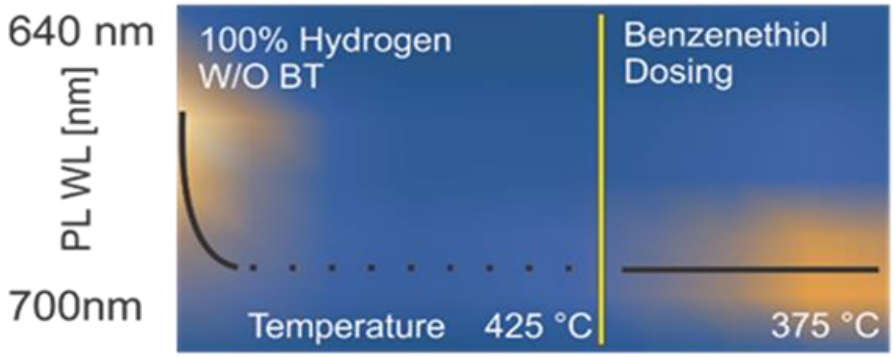

Figure 21 Mean intensity of PL of triangle is plotted over time and measured at -100°C. PL gets dimmed after 2 hours elevated at 425°C. After 10 hours, Benzenethiol is introduced at lower temperature of 375 °C and measured at -100°C. PL is recovered redshifted frequency.

Comparative images for the 660 nm and 690 nm filters and for before and after dosing are magnified and shown in figure 22 a), b), c), d) and boxed in blue and red in figure 21. The patterns of images are different for both frequencies before and after benzenethiol dosing. After 2 hours, the PL intensities are dimmed, and the defect density state is past enhancement PL peak to the defect rich side. And at this point the transformation of the pattern has been taken places. Recovery pattern shows more of the basal plane recovery than the edge recovery. Both edge and basal plane is on the rich defect density side and dosing can be done to repair structure to make its density closer to PL enhancement peaks.

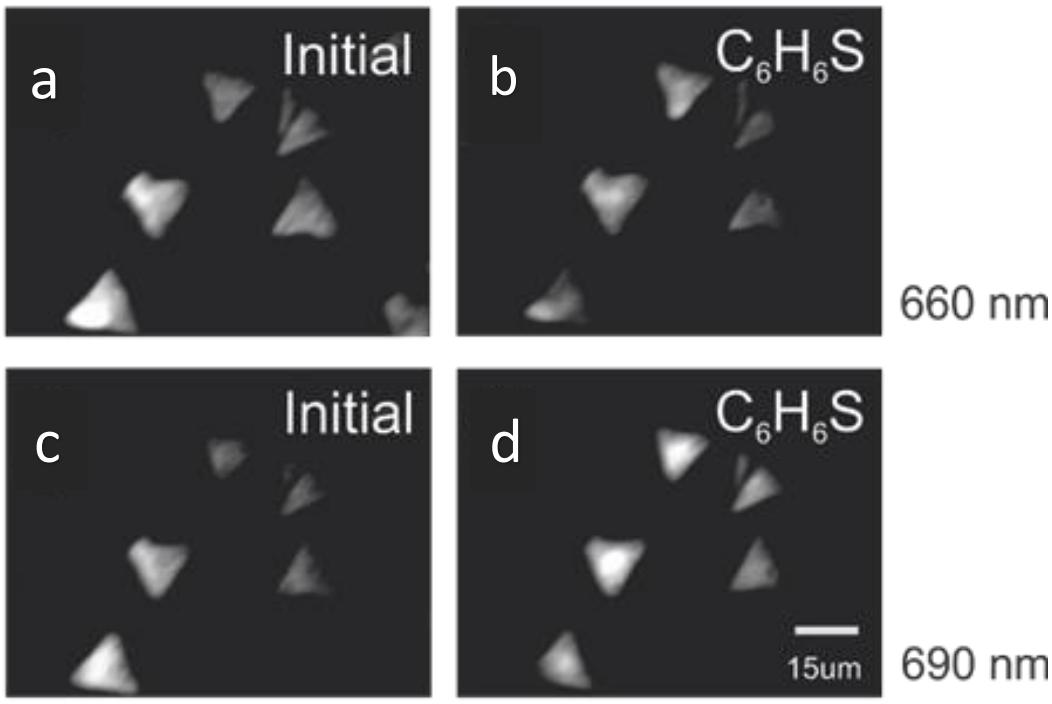

Figure 22 initial condition PL images for 660nm and 690nm denoted a and c, and after dosing benzenethiol at 375°C for the same frequency denoted b, d respectively measured at -100°C

Comparing the PL image pattern of an elevated temperature at 425°C in figure 24, they are different from the pristine condition and from the benzenethiol recovered PL pattern. The edge feature is almost gone, and only a very dimmed basal plane is observed. You can infer the movement of structure in basal plane is associated with defects in this temperature regime. For low-temperature processed PL images, the PL patterns are not altered from pristine, but the memory red-shifting has been observed for all temperatures except 425°C. The structure is not altered in basal plane. The

dynamic-state PL images show real-time surface PL morphology without changes associated to just temperature change.

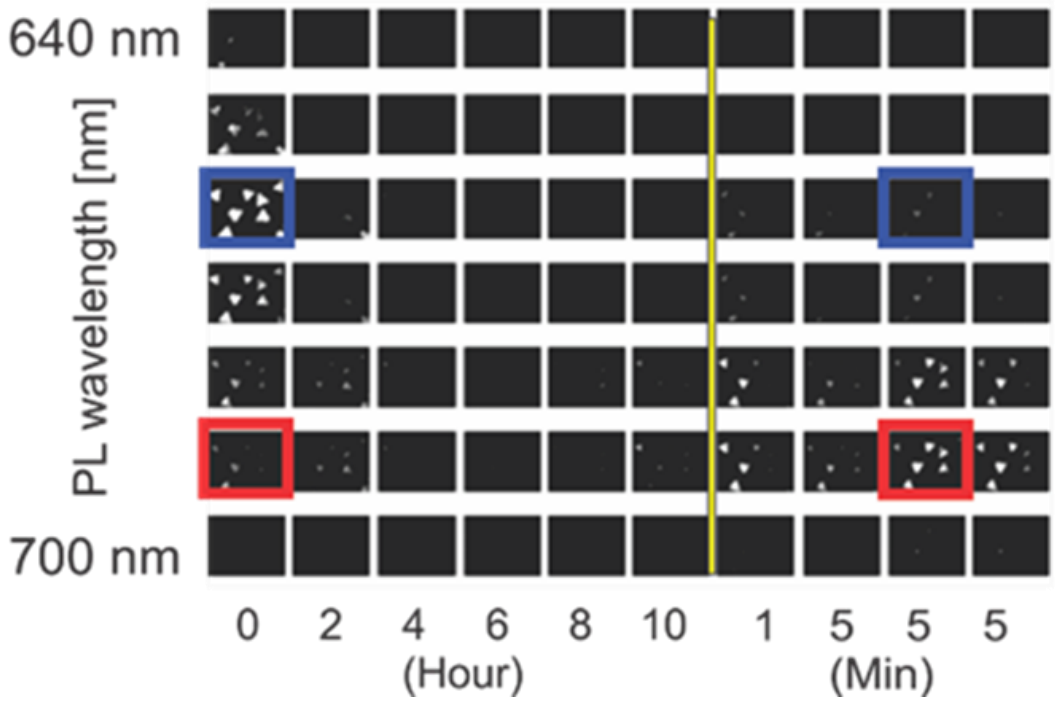

figure 23 Actual PL images corresponding to the PL intensity plot on figure 20. The sample is heated up to 425°C followed by Benzenethiol dosing process at 375°C. Zoomed in images a), c) of figure 22 for 660 nm initial and after dosing Benzenethiol boxed in blue and zoomed in images for 690nm boxed in red in b), d) in figure 22 for initial and after dosing Benzenthiol.

The next chapter discusses what happens to the PL patterns when dosing benzenethiol at the HDS relevant temperature. When it is over 425°C, it is defect rich regime on the defect density and corresponding PL intensity is dim. After Benzenethiol is dosed at 375°C, PL gets brighter. For 275°C, the defect is still lean side which took 8 hours for PL to get into defect induced PL enhancement region.

This temperature is lower end of HDS temperatures which we are not able to detect HDS activities with GC mass spectrometer.

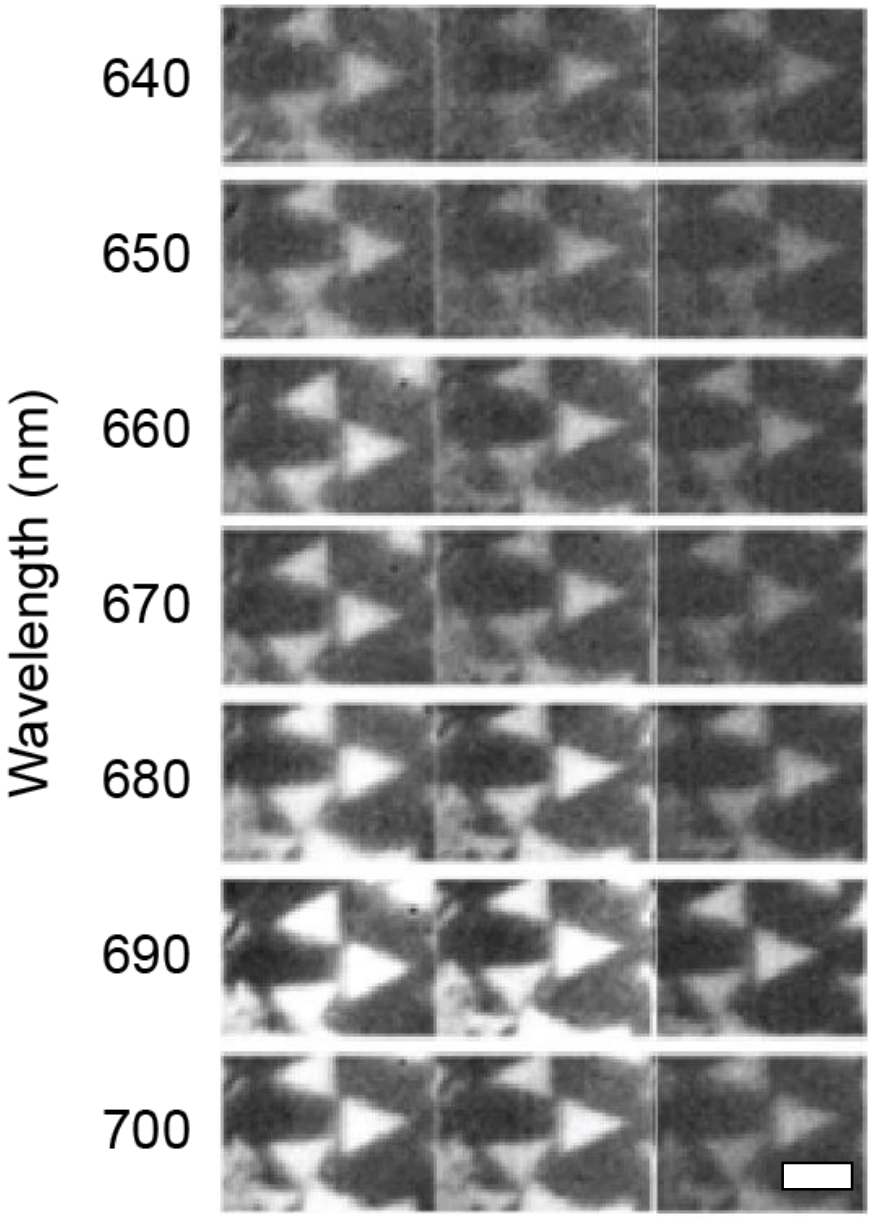

Figure 24 PL images acquired at 2, 4, and 6 hours respectively at 425°C. Peak brightness is located around 690 nm with almost no edge features. The scale bar is 15 um.

Chapter 4 PL Imaging at Dynamic Condition under Benzenethiol Dosing

4.1 Introduction

Defect induced PL enhancement may have strong correlation to HDS activities. Photoluminescence require defect site to induce recombination. Without defect with perfect crystal, recombination is too difficult because there is no electrical inhomogeneity to unbalance exciton pairs. Likewise, HDS catalysis also involves electrical imbalance from sulfur vacancy defect and the polar property of benzenethiol. Studying PL at HDS elevated temperatures under dynamic conditions will give us further understanding of the mechanism relevant to photoluminescence behavior and HDS mechanism.

In order to understand the spatial information for MoS_2 catalytic activity, we performed three different benzenethiol dosing experiments. Two experiments are at temperatures of 250°C and 300°C, which is the pre-HDS regime and another experiment is at the HDS active temperature of 370°C. We expected to recover PL intensity while dosing benzenethiol in both temperatures, and indeed recovery is observed in both cases. Past research for MoS_2 catalysis has suggested that vacancy sites are poisoned by hydrogen sulfide especially at the basal plane and concludes that the edge sites are the main, if not only, place that catalysis is taking place. Currently, people who are studying hydrogen evolution catalysis claim that both the basal plane as well as the edges are responsible for water splitting catalysis. Water splitting takes place below boiling

temperature so the mechanism catalysis may be different from elevating temperature to 300°C to 400°C. Is it the similar case for HDS catalysis? Hydrogen sulfide is produced at the sample surface as well as on most of the hot metal surface. This is because sulfur is provided by benzenethiol to the hydrogen gases. H_2S has a strong binding affinity to the basal-plane vacancy sites as studied in STM research, thus this poisoning effect inhibits catalysis on the MoS_2 surfaces. Benzenethiol may also poison the catalytic sites if there is not enough energy to create additional vacancies. The condition in order to have a continuous HDS reaction is that the rate of adsorption and desorption of functional sulfur must be at least equal to each other or the desorption of sulfur has to be much greater. At the HDS active temperature regime, we have studied the PL intensity changes while dosing benzenethiol at elevated temperatures in order to relate how the catalysis is taking place on the MoS_2 surface.

4.2 Materials and Methods

For this experiment, we used CVD grown MoS_2 islands on a 300 nm SiO_2 substrate. The sample chamber is maintained at 760 Torr with hydrogen flow at 500 sccm and chamber has total volume of approximately 5000 $_{cm}{}^3$. While the sample temperature is elevated and maintained at 250°C, there is continuous dosing of benzenethiol via bubbling through nitrogen gas with a flow-rate of 50 sccm. The leak valve is then opened for 60 seconds, and the PL images are immediately taken just before dosing benzenethiol and just after dosing.

For the second experiment, we measure the mean PL intensity at 300°C while dosing benzenethiol. The pressure of the main chamber is maintained at 760 Torr with 100 Torr hydrogen and 600 Torr nitrogen with a constant flow rate to balance the exhausting rate. The temperature is maintained at 300°C under this condition for over 12 hours total. Mean PL intensity is determined by PL imaging continuously. Once the PL intensity reaches its lowest point, benzenethiol is introduced. Once the PL brightness begins to saturate, the dosing is ceased. We continue to measure PL intensity continuously until the PL brightness starts to decrease again to the lowest saturation level.

The third experiment design has a similar procedure to the previous experiments and is done at 370°C while the mass spectrometer simultaneously acquires masses 110, 78, and 34 for benzenethiol, benzene, and hydrogen sulfide respectively. The PL images are acquired as fast as manually possible due the difficulty of focusing of images at elevated temperatures which are unstable. Periodic manual focusing is necessary to obtain clear images prior to acquiring the PL wide-field images.

4.3 Results and Discussion

At 250°C, while dosing benzenethiol, the overall PL intensity increases and both the edge and basal plane PL recover. Also, the PL brightness does not fluctuate as much after the PL intensity increases. Both figure 25 images c) and d)

are on the same brightness scale showing how the PL brightness has increased. Figure 25 a) shows overall experimental setup and b) shows PL intensity at room temperature. In comparing the initial PL image b) at room temperature and after dosing with benzenethiol d), a similar area recovers its brightness with only a few exceptions. In some cases, recovery is only taking place at the centers of the triangles. We do not observe a rapid decrease of PL intensity neither during nor after the benzenethiol dosing. A similar experimental condition is carried out with a mass spectrometer as discussed in chapter 2.

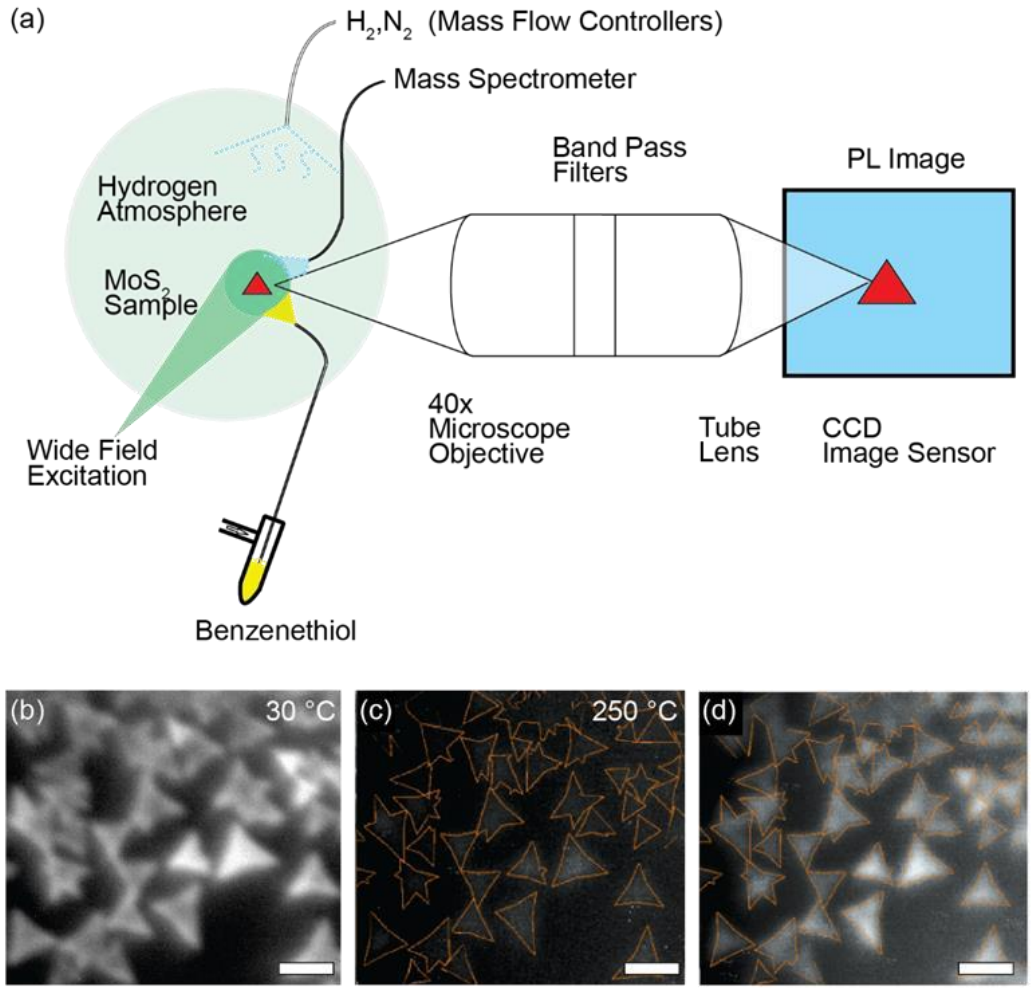

Figure 25 The overall schematic with benzenethiol dosing setup in a) with benzenethiol delivered by 1 mm ID stainless steel tubing next to the sample. Simplified PL microscope set up is shown as well. Initial PL image at room temperature is shown in b). PL intensity is diminished at 250°C under hydrogen environment in c) and benzenethiol is introduced to recover PL intensity shown at d). Some of the triangle patterns of PL recovery may be different from initial condition. The scale bar is 15 um.

Based on the experiment for measuring HDS activity, 250°C is too low of a temperature for continuous HDS to take place. After elevating temperature, we wait until PL intensity is stabilized using an hourly scale so that excessive sulfur is

desorbed. We see brightness has been recovered to some extent so therefore, the defect density is at rich side of the PL brightness profile. Benzenethiol makes the MoS_2 triangles respond closer to the PL defect enhancement regime.

It takes six hours to get the lowest PL intensity mean under the hydrogen gas environment at 300°C. It takes two hours for PL brightness to recover from the lowest to mid intensity range via benzenethiol dosing. It takes another two hours for the PL intensity to reach its lowest point when benzenethiol is not supplied as seen in figure 26. The initial slope of decay and the slope of decay after the benzenethiol recovery are both similar. If the surface of MoS_2 triangles and film are the only active catalytic sites, then the adsorption and desorption rate associated with the PL intensity are too slow for the mass spectrometer to detect any HDS activities. The response of PL brightness with benzenethiol dosing needs to be faster in order for the HDS activity to be detected on the mass spectrometer. After the first 6 hours, the defect density is at rich side of the PL intensity profile and dosing with benzenethiol brings it back closer to PL enhancement regime. Since the mass spectrometer measurement does not confirm the HDS activity at 300°C, we elevated the temperature regime for the PL imaging experiment in the following series.

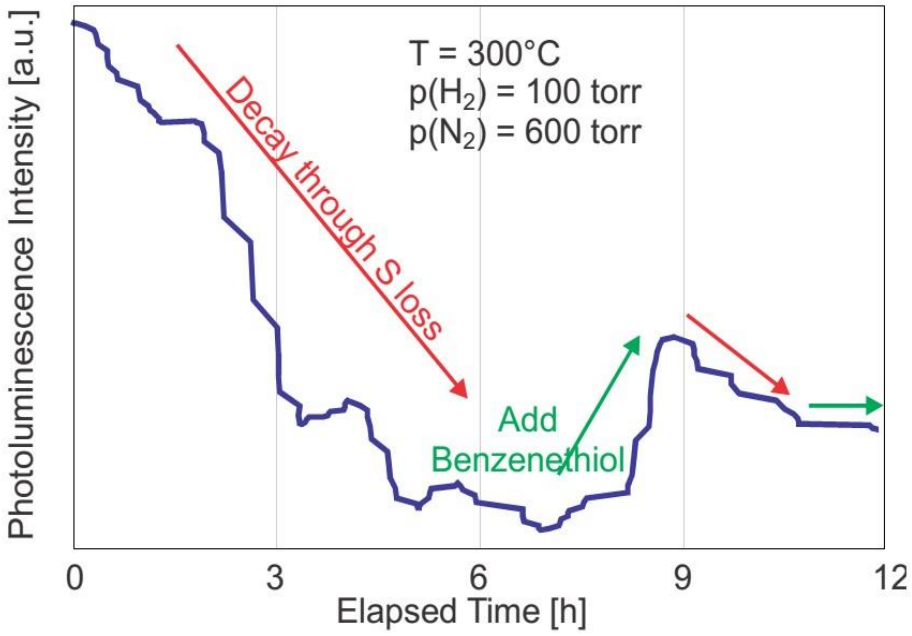

Figure 26 PL intensity of an MoS_2 island during exposure to 100 torr of H_2 at 300°C. After a short initiation phase (not shown), a continuous decrease of PL intensity is visible, which is partially recovered when at 7h and 8h increasing bursts of benzenethiol are added to the process gas. Subsequently, the PL starts to decrease again, until at 11 hour, BT is leaked continuously into the process gas to stabilize film conditions.

The HDS activity on the MoS_2 films is confirmed with gas chromatography and mass spectrometry at 360°C as discussed on chapter 2. PL recovery takes place and the brightness increases at the exact moment that benzenethiol is introduced at 370°C. This brightness-recovered PL image #4 is different PL image #3 before start dosing Benzenthiol and post PL image #5 in figure 27 a). Soon after, the PL pattern begins to go back to the shape it was before the benzenethiol was dosed . The brightness gets continuously dimmer during the 16-minute interval of next PL image acquisition as seen in the next PL image in figure 27 a), despite continuously dosing benzenethiol. The HDS activity is

highest at position #4 for short a duration when the PL images are brighter at #4 on figure 27 a) and b) .

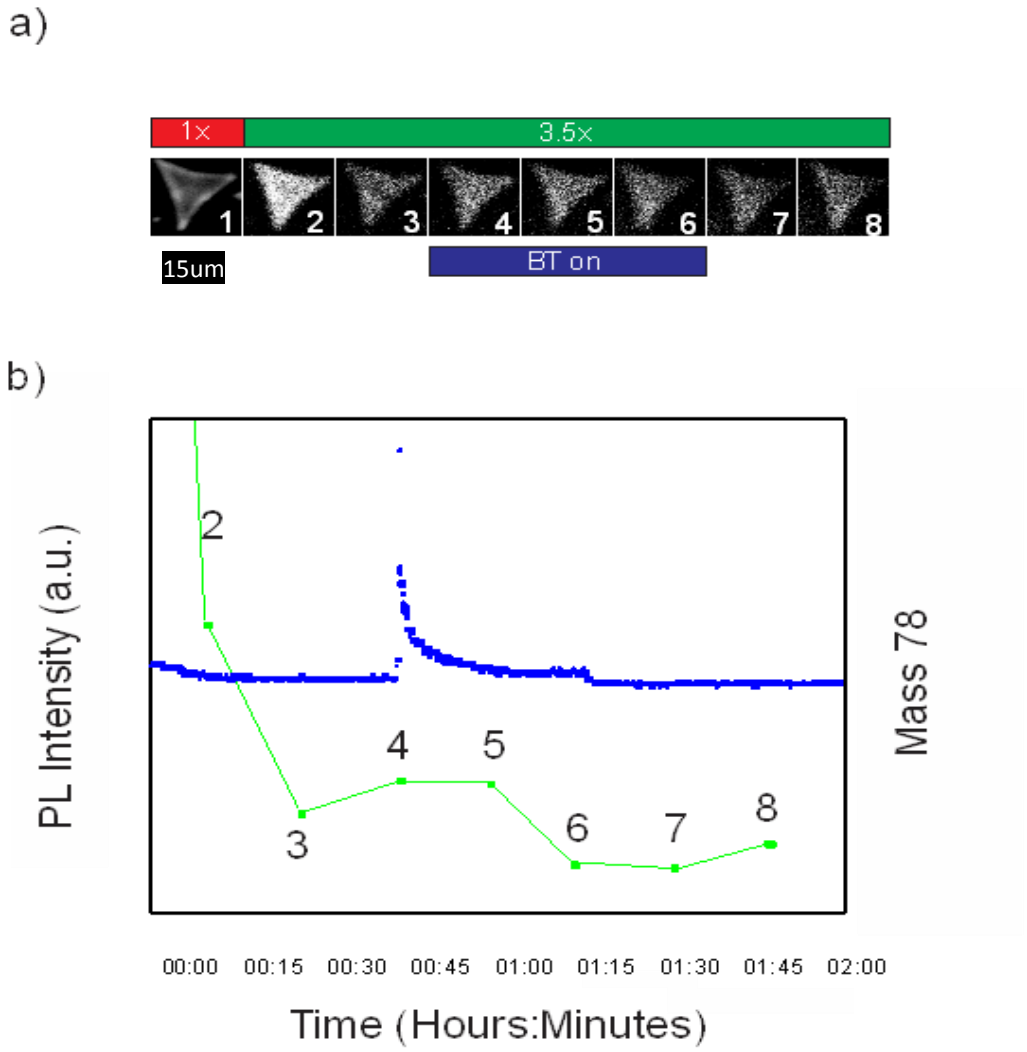

Figure 27 Series of PL images maintained at 370°C are shown in a). The intensity of images are magnified by a scale bar on top to show clear pattern. Mean intensity of the corresponding images are shown on green plot on b). Rapid decrease of PL intensity within 15 minutes of holding 370°C which indicates rapid desorption of sulfur on the surface. Blue Line indicates the benzene (mass 78) concentration with rapid increases with benzenethiol dosing from 35 min to 70 min. Initial rapid increase of PL intensity is not maintained and starts to decrease despite continuous dosing. This instability is similar to the experiment at 300°C however it is much shorter time scale at higher temperature. At image 6, it is still continuously dosing benzenethiol, but PL intensity decrease to the stable bottom similar to image 7 and after stop dosing benzenethiol. Therefore, regardless of constant supply of sulfur, strong desorption is dominating over adsorption. Initially edge is prominent, it becomes featureless pattern on the basal plane of the sample at elevated temperature. This flat region changes its PL brightness momently when Benzenethiol is dosing but it stabilized to lower PL brightness. All observable PL activities at this temperature is at basal plane.

The defect density must be on the rich side and for the moment, the defect has been decreased and PL gets brighter for one attempt. The PL recovery amount is small as one can predict that slop at 370°C on figure 10 is very flat. Whereas at 250°C and 300°C, PL slope is steeper which corresponding to greater PL increases with Benzenethiol dosing. For the same sample, long after the PL image brightness reaches its lowest point (in the 2-hour duration) and the dosing for the second time for the same sample at the same temperature is complete, we observe that the PL brightness does not recover. However, the HDS activity peak resembles the pristine sample which undergoes the first benzenethiol dosing. This may be because defect density remains on a similar rich level on the surface. A similar result takes place for the sample at 360°C which is not shown here. While dosing benzenethiol at these elevated temperatures, the edge feature PL recovery is not observed for the second attempt. Well beyond far elevated temperatures, the defect regime is too rich and thus recovery may not be observable.

Thanks to the PL enhancement due to defects which act as a lighthouse of defect density around HDS relevant temperature. We can infer additional defect information in addition to the standard temperature induced decay. PL patterns shape like the mountain profile shown for the moment that benzenethiol is introduced at 370°C on samples with MoS_2 triangles. The change of PL intensity occurring in this shape means that the defect density fluctuates in this pattern.

Edge defects may also be fluctuating but not to the PL enhancement regime at this temperature therefore it is not able to be observed. One can infer from this that the entire mountain surface contributes as an active catalytic site with the bottom having higher desorption, and the top having slightly lower desorption. Up to 375°C the PL pattern maintains its shape from the pristine sample discussed in chapter 3. At temperatures over 425°C, the PL pattern begins to change into a mountain shape pattern measured at a frozen state at -100°C. It seems as though MoS_2 triangles formed via CVD growth have less defects in the center and more towards the edges. Edges are chemically truncated while the basal plane is surrounded by complete neighbors. Therefore, the edges are more defect rich than the basal plane. The PL intensity fluctuation is on the minute time-scale for HDS to be detectable on the mass spectrometer. It must be on the minute time-scale or we can infer that continuous HDS may not be taking place. For MoS_2 HDS catalysis, it is not limited to edge site activity because there are basal plane sites that are catalytically active observed using our wide-field PL imaging method and confirmed with gas chromatography and mass spectrometry.

5.0 Conclusion

Our wide-field PL imaging method shows microscopic transition of surface conditions of monolayer MoS_2 relevant to HDS catalysis. H_2S is continuously detected in HDS temperature regime from 200°C to 400°C with the continuous

sampling method. For the gas chromatography sampling technique, the temperature is over 340°C. In the pre-HDS temperature regime around 200°C to 300°C, the PL images show enhancement in PL intensity and a red-shifting effect due to an increase in defect density and a thermally induced physical stretch of the MoS_2 film. The GC mass spectrometer may not be sensitive enough and thus many triangles are needed to detect HDS activity at the edges for this lower temperature regime. We have observed a PL enhancement in this temperature regime, which is a similar result from the previous STM and TEM publications. There is movement of sulfur atoms on the edges. In the frozen-state PL measurements, there is a PL red-shift memory effect in this temperature regime. However, right at the HDS active temperature starting at around 340°C in our setup, the PL edge feature is gone but the basal plane pattern remains. At temperatures over 425°C, the PL is dimmed at low temperature measurement and benzenethiol dosing at the lower temperature recovers its PL pattern completely which is different from that of the pattern at the initial condition. Some movement of structure at the basal plane is inferred from this. The dimming rate of PL intensity is compared at different temperature regimes. As temperature is approaches the actual industrial processing temperature, the PL dimming rate is on the minute time-scale for HDS active temperatures, compared to the hour time-scales for that of pre-HDS temperature measurements. The standard hydrocracking process in industry uses temperatures between 360° and 420°C, as

extracted from the figure in this handbook[71]. There are in situ studies using STM and TEM on the atomic scale with elevated temperatures around 200°C. Temperatures in that study were not able to reach industrial processing temperatures due to instrumentational limitations. Our PL imaging technique shows density fluctuation activity on not only edge sites but also on basal plane sites. Focusing solely on the edge activities at lower-than-actual HDS process temperatures may prevent the understanding of the true main contributing catalytic mechanism.

Reference

1. Mak, K.; Lee, C.; Hone, J.; Shan, J.; Heinz, T., Atomically Thin MoS2: A New Direct-Gap Semiconductor. *Physical Review Letters* **2010,** *105* (13).

2. Li, G.; Zhang, D.; Qiao, Q.; Yu, Y.; Peterson, D.; Zafar, A.; Kumar, R.; Curtarolo, S.; Hunte, F.; Shannon, S.; Zhu, Y.; Yang, W.; Cao, L., All The Catalytic Active Sites of MoS2 for Hydrogen Evolution. **2016**.

3. Zhou, Q.; Su, S.; Hu, D.; Lin, L.; Yan, Z.; Gao, X.; Zhang, Z.; Liu, J., Ultrathin MoS2-coated Ag@Si nanosphere arrays as an efficient and stable photocathode for solar-driven hydrogen production. *Nanotechnology* **2018,** *29* (10).

4. Chen, R.; Wang, P.; Chen, J.; Wang, C.; Ao, Y., Synergetic effect of MoS2 and MXene on the enhanced H-2 evolution performance of CdS under visible light irradiation. *Applied Surface Science* **2019,** *473*, 11-19.

5. Rao, C.; Lingampalli, S.; Dey, S.; Roy, A., Solar photochemical and thermochemical splitting of water. *Philosophical Transactions of the Royal Society a-Mathematical Physical and Engineering Sciences* **2016,** *374* (2061).

6. Wei, H.; Yang, Z.; Min, Y.; Fan, J.; Xu, Q., Light Auxiliary Hydrogen-Evolution Catalyst Based on Uniformly Pt Nanoparticles Decorated Molybdenum Sulfide Hybrids. *Particle & Particle Systems Characterization* **2017,** *34* (3).

7. Joshi, R.; Shukla, S.; Saxena, S.; Lee, G.; Sahajwalla, V.; Alwarappan, S., Hydrogen generation via photoelectrochemical water splitting using chemically exfoliated MoS2 layers. *Aip Advances* **2016,** *6* (1).

8. Gupta, U.; Rao, C., Hydrogen generation by water splitting using MoS2 and other transition metal dichalcogenides. *Nano Energy* **2017,** *41*, 49-65.

9. Alqahtani, M.; Sathasivam, S.; Cui, F.; Steier, L.; Xia, X.; Blackman, C.; Kim, E.; Shin, H.; Benamara, M.; Mazur, Y.; Salamo, G.; Parkin, I.; Liu, H.; Wu, J., Heteroepitaxy of GaP on silicon for efficient and cost-effective photoelectrochemical water splitting. *Journal of Materials Chemistry a* **2019,** *7* (14), 8550-8558.

10. Song, Y.; Wei, S.; Rong, Y.; Lu, C.; Chen, Y.; Wang, J.; Zhang, Z., Enhanced visible-light photocatalytic hydrogen evolution activity of Er3+:Y3Al5O12/PdS-ZnS by conduction band cocatalysts (MoO2, MoS2 and MoSe2). *International Journal of Hydrogen Energy* **2016,** *41* (30), 12826-12835.

11. Yuan, Y.; Chen, D.; Yang, S.; Yang, L.; Wang, J.; Cao, D.; Tu, W.; Yu, Z.; Zou, Z., Constructing noble-metal-free Z-scheme photocatalytic overall water splitting systems using MoS2 nanosheet modified CdS as a H-2 evolution photocatalyst. *Journal of Materials Chemistry a* **2017,** *5* (40), 21205-21213.

12. Parija, A.; Choi, Y.-H.; Liu, Z.; Andrews, J. L.; Jesus, L. R. D.; Fakra, S. C.; Al-Hashimi, M.; Batteas, J. D.; Prendergast, D.; Banerjee, S., Mapping Catalytically Relevant Edge Electronic States of MoS2. **2018**.

13. Besenbacher, F.; Brorson, M.; Clausen, B.; Helveg, S.; Hinnemann, B.; Kibsgaard, J.; Lauritsen, J.; Moses, P.; Norskov, J.; Topsoe, H., Recent STM, DFT and HAADF-STEM studies of sulfide-based hydrotreating catalysts: Insight into mechanistic, structural and particle size effects. *Catalysis Today* **2008,** *130* (1), 86-96.

14. Dinter, N.; Rusanen, M.; Raybaud, P.; Kasztelan, S.; da Silva, P.; Toulhoat, H., Temperature-programmed reduction of unpromoted MoS2-based hydrodesulfurization catalysts: First-principles kinetic Monte Carlo simulations and comparison with experiments.
Journal of Catalysis **2010,** *275* (1), 117-128.

15. Helveg, S.; Lauritsen, J. V.; Laegsgaard, E.; Stensgaard, I. I.; Norskov, J. K.; Clausen, B. S.; Topsoe, H.; Besenbacher, F., Atomic-scale structure of single-layer MoS2 nanoclusters. *Phys Rev Lett* **2000,** *84* (5), 951-4.

16. Hansen, L. P.; Ramasse, Q. M.; Kisielowski, C.; Brorson, M.; Johnson, E.; Topsoe, H.; Helveg, S., Atomic-scale edge structures on industrial-style MoS2 nanocatalysts. *Angew Chem Int Ed Engl* **2011,** *50* (43), 10153-6.

17. Zhu, Y.; Ramasse, Q.; Brorson, M.; Moses, P.; Hansen, L.; Kisielowski, C.; Helveg, S., Visualizing the Stoichiometry of Industrial-Style Co-Mo-S Catalysts with Single-Atom Sensitivity.
Angewandte Chemie-International Edition **2014,** *53* (40), 10723-10727.

18. Zhu, S.; Wang, Q., A simple method for understanding the triangular growth patterns of transition metal dichalcogenide sheets. **2015**.

19. Moses, P.; Hinnemann, B.; Topsoe, H.; Norskov, J., The effect of Co-promotion on MoS2 catalysts for hydrodesulfurization of thiophene: A density functional study. *Journal of Catalysis* **2009,** *268* (2), 201-208.

20. Durnev, M.; Glazov, M., Excitons and trions in two-dimensional semiconductors based on transition metal dichalcogenides. *Physics-Uspekhi* **2018,** *61* (9), 825-845.

21. Lembke, D.; Bertolazzi, S.; Kis, A., Single-Layer MoS2 Electronics. *Accounts of Chemical Research* **2015,** *48* (1), 100-110.

22. Rahman, I.; Purqon, A.; Waris, A.; Shin, B.; Kondo, M.; Buys, Y.; Irwanto, D.; Pramuditya, S., First Principles Study of Molybdenum Disulfide Electronic Structure. *International Conference on Energy Sciences (Ices 2016)* **2017,** *877*.

23. Splendiani, A.; Sun, L.; Zhang, Y.; Li, T.; Kim, J.; Chim, C.; Galli, G.; Wang, F., Emerging Photoluminescence in Monolayer MoS2. *Nano Letters* **2010,** *10* (4), 1271-1275.

24. Wang, B.; Yang, S.; Chen, J.; Mann, C.; Bushmaker, A.; Cronin, S., Radiation-induced direct bandgap transition in few-layer MoS2. *Applied Physics Letters* **2017,** *111* (13).

25. Zhao, H.; Mao, X.; Zhou, D.; Feng, S.; Shi, X.; Ma, Y.; Wei, X.; Mao, Y., Bandgap modulation of MoS2 monolayer by thermal annealing and quick cooling. *Nanoscale* **2016,** *8* (45), 18995-19003.

26. Wang, S.; Rong, Y.; Fan, Y.; Pacios, M.; Bhaskaran, H.; He, K.; Warner, J. H., Shape Evolution of Monolayer MoS2 Crystals Grown by Chemical Vapor Deposition. **2014**.

27. Li, H.; Zhu, X.; Tang, Z.; Zhang, X., Low-temperature photoluminescence emission of monolayer MoS2 on diverse substrates grown by CVD. *Journal of Luminescence* **2018,** *199*, 210215.

28. Koh, E.; Chiu, C.; Lim, Y.; Zhang, Y.; Pan, H., Hydrogen adsorption on and diffusion through MoS2 monolayer: First-principles study. *International Journal of Hydrogen Energy* **2012,** *37* (19), 14323-14328.

29. Mann, J. C., Synthesis and characterization of few layer semiconducting transition metal dichalcogenides. University of California, Riverside,: Riverside, California, 2013; p. 1 online resource (74 pages). Online version UC access only http://search.proquest.com/docview/1500827522?accountid=14521.

30. Hu, Y.; Zhang, F.; Titze, M.; Deng, B.; Li, H.; Cheng, G. J., Straining effects in MoS2 monolayer on nanostructured substrates: temperature-dependent photoluminescence and exciton dynamics. *Nanoscale* **2018,** *10* (12), 5717-5724.

31. Lanzillo, N.; Birdwell, A. G.; Amani, M.; Crowne, F. J.; Shah, P. B.; Najmaei, S.; Liu, Z.; Ajayan, P. M.; Lou, J.; Dubey, M.; Nayak, S. K.; O'Regan, T. P., Temperature-dependent Phonon Shifts in Monolayer MoS2. **2013**.

32. Aas, S.; Bulutay, C., Strain dependence of photoluminescence and circular dichroism in transition metal dichalcogenides: a k . p analysis. *Optics Express* **2018,** *26* (22), 28672-28681. 33.

33. Bai, S.; Niu, C.; Yu, W.; Zhu, Z.; Cai, X.; Jia, Y., Strain Tunable Bandgap and High Carrier Mobility in SiAs and SiAs2 Monolayers from First-Principles Studies. *Nanoscale Research Letters* **2018,** *13*.

34. Castellanos-Gomez, A.; Roldan, R.; Cappelluti, E.; Buscema, M.; Guinea, F.; van der Zant, H.; Steele , G., Local Strain Engineering in Atomically Thin MoS2. *Nano Letters* **2013,** *13*(11), 5361-5366.

35. Conley, H.; Wang, B.; Ziegler, J.; Haglund, R.; Pantelides, S.; Bolotin, K., Bandgap Engineering of Strained Monolayer and Bilayer MoS2. *Nano Letters* **2013,** *13* (8), 3626-3630.

36. Deng, S.; Zhang, Y.; Li, L., Study of the strain effect on the monolayer MoS2. *2017 Ieee 17th International Conference on Nanotechnology (Ieee-Nano)* **2017**, 918-920.

37. Garcia, A.; del Corro, E.; Kalbac, M.; Frank, O., Tuning the electronic properties of monolayer and bilayer transition metal dichalcogenide compounds under direct out-of-plane compression. *Physical Chemistry Chemical Physics* **2017,** *19* (20), 13333-13340.

38. Han, G.; Tu, K.; Niroui, F.; Xu, W.; Zhou, S.; Wang, X.; Bulovic, V.; Ross, C.; Warner, J.; Grossman, J., Photoluminescent Arrays of Nanopatterned Monolayer MoS2. *Advanced Functional Materials* **2017,** *27* (45).

39. Conley, H. J.; Wang, B.; Ziegler, J. I.; Richard F. Haglund, J.; Pantelides, S. T.; Bolotin, K. I., Bandgap Engineering of Strained Monolayer and Bilayer MoS2. **2013**.

40. Mom, R. V.; Louwen, J. N.; Frenken, J. W. M.; Groot, I. M. N., In situ observations of an active MoS 2 model hydrodesulfurization catalyst. *Nature Communications* **2019,** *10* (1), 1-8. 41.

41. Bruix, A.; Fuchtbauer, H.; Tuxen, A.; Walton, A.; Andersen, M.; Porsgaard, S.; Besenbacher, F.; Hammer, B.; Lauritsen, J., In Situ Detection of Active Edge Sites in Single-Layer MoS2 Catalysts. *Acs Nano* **2015,** *9* (9), 9322-9330.

42. Besenbacher, F.; Lauritsen, J.; Linderoth, T.; Laegsgaard, E.; Vang, R.; Wendt, S., Atomicscale surface science phenomena studied by scanning tunneling microscopy. *Surface Science* **2009,** *603* (10-12), 1315-1327.

43. Besenbacher, F.; Thostrup, P.; Salmeron, M., The structure and reactivity of surfaces revealed by scanning tunneling microscopy. *Mrs Bulletin* **2012,** *37* (7), 677-681.

44. Helveg, S.; Lauritsen, J.; Laegsgaard, E.; Stensgaard, I.; Norskov, J.; Clausen, B.; Topsoe, H.; Besenbacher, F., Atomic-scale structure of single-layer MoS2 nanoclusters. *Physical Review Letters* **2000,** *84* (5), 951-954.

45. Kushmerick, J.; Kandel, S.; Han, P.; Johnson, J.; Weiss, P., Atomic-scale insights into hydrodesulfurization. *Journal of Physical Chemistry B* **2000,** *104* (14), 2980-2988.

46. Lauritsen, J.; Bollinger, M.; Laegsgaard, E.; Jacobsen, K.; Norskov, J.; Clausen, B.; Topsoe, H.; Besenbacher, F., Atomic-scale insight into structure and morphology changes of MoS2 nanoclusters in hydrotreating catalysts. *Journal of Catalysis* **2004,** *221* (2), 510-522.

47. Lauritsen, J.; Vang, R.; Besenbacher, F., From atom-resolved scanning tunneling microscopy (STM) studies to the design of new catalysts. *Catalysis Today* **2006,** *111* (1-2), 34-43.

48. Lauritsen, J.; Besenbacher, F., Atom-resolved scanning tunneling microscopy investigations of molecular adsorption on MoS2 and CoMoS hydrodesulfurization catalysts.
Journal of Catalysis **2015,** *328*, 49-58.

49. Marion, I.; Capeta, D.; Pielic, B.; Faraguna, F.; Gallardo, A.; Pou, P.; Biel, B.; Vujicic, N.; Kralj, M., Atomic-scale defects and electronic properties of a transferred synthesized MoS2 monolayer. *Nanotechnology* **2018,** *29* (30).

50. Nan, H.; Wang, Z.; Wang, W.; Liang, Z.; Lu, Y.; Chen, Q.; He, D.; Tan, P.; Miao, F.; Wang, X.; Wang, J.; Ni, Z., Strong Photoluminescence Enhancement of MoS2 through Defect Engineering and Oxygen Bonding. **2014**.

51. Wu, K.; Li, Z.; Tang, J.; Lv, X.; Wang, H.; Luo, R.; Liu, P.; Qian, L.; Zhang, S.; Yuan, S., Controllable defects implantation in MoS2 grown by chemical vapor deposition for photoluminescence enhancement. *Nano Research* **2018,** *11* (8), 4123-4132.

52. Andrzejewski, D.; Marx, M.; Grundmann, A.; Pfingsten, O.; Kalisch, H.; Vescan, A.; Heuken, M.; Kummell, T.; Bacher, G., Improved luminescence properties of MoS2 monolayers grown via MOCVD: role of pretreatment and growth parameters. *Nanotechnology* **2018,** *29* (29).

53. Kaplan, D.; Gong, Y.; Mills, K.; Swaminathan, V.; Ajayan, P.; Shirodkar, S.; Kaxiras, E., Excitation intensity dependence of photoluminescence from monolayers of MoS2 and WS2/MoS2 heterostructures. *2d Materials* **2016,** *3* (1).

54. Nan, H.; Wang, Z.; Wang, W.; Liang, Z.; Lu, Y.; Chen, Q.; He, D.; Tan, P.; Miao, F.; Wang, X.; Wang, J.; Ni, Z., Strong Photoluminescence Enhancement of MoS2 through Defect Engineering and Oxygen Bonding. *Acs Nano* **2014,** *8* (6), 5738-5745.

55. Siyaram, S.; Hanbicki, A.; Rosenberger, M.; Jernigan, G.; Chuang, H.; McCreary, K.; Jonker, B., Spatially Selective Enhancement of Photoluminescence in MoS2 by Exciton-Mediated Adsorption and Defect Passivation. *Acs Applied Materials & Interfaces* **2019,** *11* (17), 1614716155.

56. Su, W.; Jin, L.; Qu, X.; Huo, D.; Yang, L., Defect passivation induced strong photoluminescence enhancement of rhombic monolayer MoS2. *Physical Chemistry Chemical Physics* **2016,** *18* (20), 14001-14006.

57. Tongay, S.; Suh, J.; Ataca, C.; Fan, W.; Luce, A.; Kang, J.; Liu, J.; Ko, C.; Raghunathanan, R.; Zhou, J.; Ogletree, F.; Li, J.; Grossman, J.; Wu, J., Defects activated photoluminescence in twodimensional semiconductors: interplay between bound, charged, and free excitons. *Scientific Reports* **2013,** *3*.

58. Almeida, K.; Wurch, M.; Geremew, A.; Yamaguchi, K.; Empante, T. A.; Valentin, M. D.; Gomez, M.; Berges, A. J.; Stecklein, G.; Rumyantsev, S.; Martinez, J.; Balandin, A. A.; Bartels, L., High-Vacuum Particulate-Free Deposition of Wafer-Scale Mono-, Bi-, and Trilayer Molybdenum Disulfide with Superior Transport Properties. *ACS Applied Materials & Interfaces* **2018,** *10* (39), 33457-33463.

59. Kim, S.; Kim, K.; Lee, Y., Effects of dispersed MoS2 catalysts and reaction conditions on slurry phase hydrocracking of vacuum residue. *Journal of Catalysis* **2017,** *347*, 127-137.

60. Grilc, M.; Likozar, B.; Levec, J., Hydrodeoxygenation and hydrocracking of solvolysed lignocellulosic biomass by oxide, reduced and sulphide form of NiMo, Ni, Mo and Pd catalysts.
Applied Catalysis B-Environmental **2014,** *150*, 275-287.

61. Jeong, H.; Lee, Y., Comparison of unsupported WS2 and MoS2 catalysts for slurry phase hydrocracking of vacuum residue. *Applied Catalysis a-General* **2019,** *572*, 90-96.

62. Sharifvaghefi, S.; Zheng, Y., Development of a Magnetically Recyclable Molybdenum Disulfide Catalyst for Direct Hydrodesulfurization. *Chemcatchem* **2015,** *7* (20), 3397-3403.

63. Vang, R.; Lauritsen, J.; Laegsgaard, E.; Besenbacher, F., Scanning tunneling microscopy as a tool to study catalytically relevant model systems. *Chemical Society Reviews* **2008,** *37* (10), 2191-2203.

64. Topsoe, H.; Lauritsen, J.; Helveg, S.; Carlsson, A.; Brorson, M.; Clausen, B.; Norskov, J.; Besenbacher, F., Recent atomic-scale insight into hydrodesulfurization catalysts. *Abstracts of Papers of the American Chemical Society* **2001,** *221*, U310-U310.

65. Lauritsen, J.; Nyberg, M.; Norskov, J.; Clausen, B.; Topsoe, H.; Laegsgaard, E.; Besenbacher, F., Hydrodesulfurization reaction pathways on MoS2 nanoclusters revealed by scanning tunneling microscopy. *Journal of Catalysis* **2004,** *224* (1), 94-106.

66. Cheng, C.; Lu, A.; Tseng, C.; Yang, X.; Hedhili, M.; Chen, M.; Wei, K.; Li, L., Activating basal-plane catalytic activity of two-dimensional MoS2 monolayer with remote hydrogen plasma. *Nano Energy* **2016,** *30*, 846-852.

67. He, Z.; Zhao, R.; Chen, X.; Chen, H.; Zhu, Y.; Su, H.; Huang, S.; Xue, J.; Dai, J.; Cheng, S.; Liu, M.; Wang, X.; Chen, Y., Defect Engineering in Single-Layer MoS2 Using Heavy Ion Irradiation.
Acs Applied Materials & Interfaces **2018,** *10* (49), 42524-42533.

68. Johnson, A.; Cheng, F.; Tsai, Y.; Shih, C., Giant Enhancement of Defect-Bound Exciton Luminescence and Suppression of Band-Edge Luminescence in Monolayer WSe2-Ag Plasmonic Hybrid Structures. *Nano Letters* **2017,** *17* (7), 4317-4322.

69. Kim, M.; Nam, G.; Park, S.; Kim, H.; Han, G.; Lee, J.; Dhakal, K.; Leem, J.; Lee, Y.; Kim, J., Photoluminescence wavelength variation of monolayer MoS2 by oxygen plasma treatment. *Thin Solid Films* **2015,** *590*, 318-323.

70. Li, D.; Zou, Q.; Huang, X.; Golgir, H.; Keramatnejad, K.; Song, J.; Xiao, Z.; Fan, L.; Hong, X.; Jiang, L.; Silvain, J.; Sun, S.; Lu, Y., Controlled defect creation and removal in graphene and MoS2 monolayers. *Nanoscale* **2017,** *9* (26), 8997-9008.

71. Speight, J.; Speight, J., The Chemistry and Technology of Petroleum FOURTH EDITION Preface. *Chemistry and Technology of Petroleum, Fourth Edition* **2007,** *114*.

Appendices

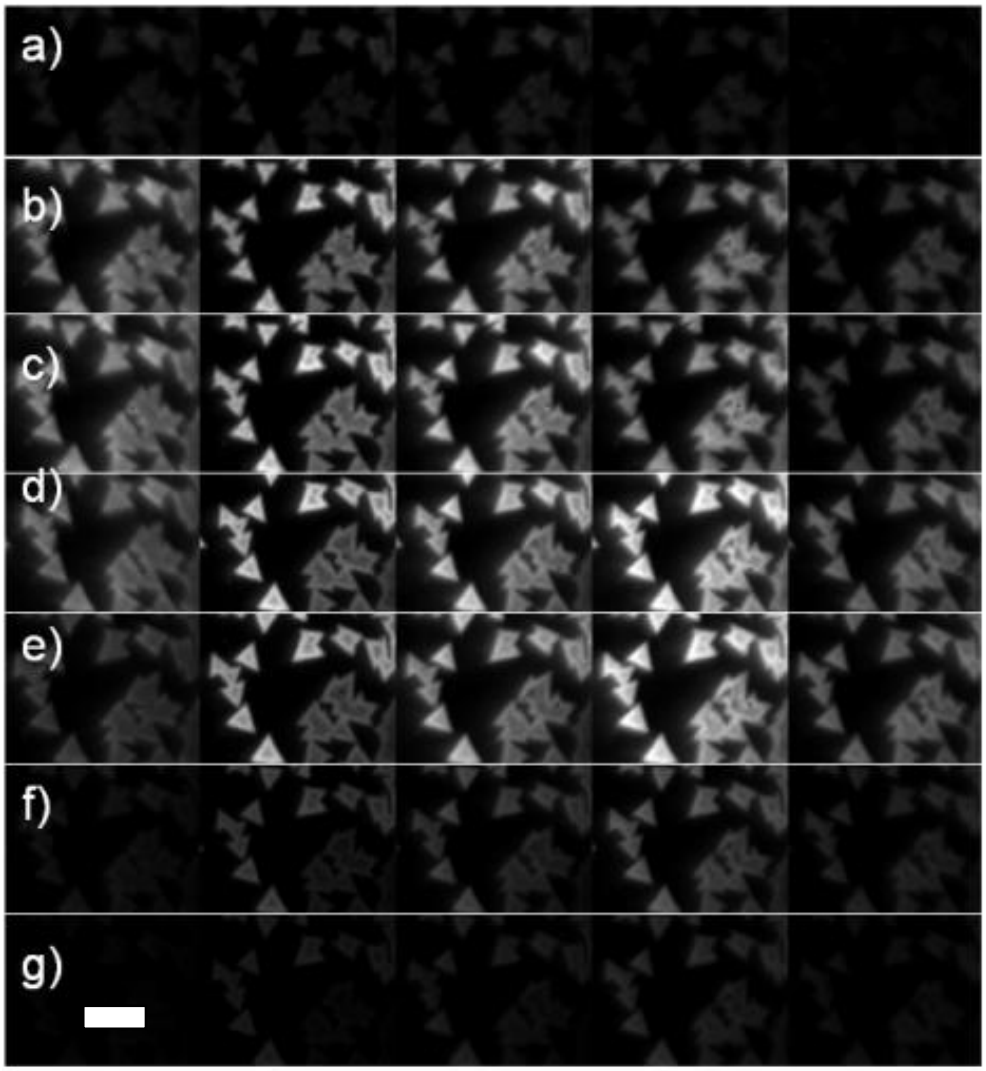

Initial **4.5 hr 310**°C **6hr 350**°C **4.5 hr 350**°C **6.5 hr 360**°C

Figure 28. PL images taken with bandpass filter with a) 650nm b) 660nm c) 670nm d) 680nm e) 690nm f) 700nm g) 710nm. Portion of these images are presented on figure 3.4-1. Bright area is believe to be in PL enhance regime with increasing defect numbers. Further processing for longer make it to be defect rich side and PL intently start to get diminishes. There may be some delay effect from dynamic PL imaging at corresponding temperature and frozen state measurement at room temperature. Red shifting of peak is observed. Shorter wavelength around 660 nm has slightly smaller PL peak perimeter compare to longer wavelength around 680nm. It may has to do with how defect size is correlated toward center from outside. Larger defects on outer region compare to smaller defects on inner region. Also PL is enhanced for certain duration which is related to PL enhancement discussed in chapter 1. The scale bar is 30 um.